# SPACE RESEARCH INSTITUTE

IWF
Space Research Institute

OAW
Austrian Academy of Sciences

# ANNUAL REPORT 2013

IWF
Space Research Institute

# ANNUAL REPORT 2013

SPACE RESEARCH INSTITUTE GRAZ
AUSTRIAN ACADEMY OF SCIENCES

ÖAW
Austrian Academy of Sciences

## Cover Image

*The Planetary Garden at the Space Research Institute: Sun, Mercury, Venus, Earth, Mars, Jupiter, and Saturn in autumn light (IWF/G. Fischer).*

# Table of Contents

# Introduction

The Space Research Institute (Institut für Weltraumforschung, IWF) of the Austrian Academy of Sciences (Österreichische Akademie der Wissenschaften, ÖAW) in Graz focuses on physics and exploration of the solar system, covering the full chain of research needed in its fields: from developing and building space-qualified instruments to analyzing and interpreting the data returned by these instruments. With over 80 staff members from more than a dozen different nationalities it is the Austrian space research institute par excellence. It cooperates closely with space agencies all over the world and with numerous other national and international research institutions. A particularly intense cooperation exists with the European Space Agency (ESA).

In terms of science, IWF concentrates on space plasma physics, on the upper atmospheres of planets and exoplanets, and on the Earth's, the Moon's, and planetary gravity fields. In the area of instrument development the focus lies on building magnetometers and on-board computers, on antenna calibration, and on satellite laser ranging.

Presently, the institute is involved in sixteen international space missions:

- *BepiColombo* will be launched in 2016 to investigate planet Mercury, using two orbiters, one specialized in magnetospheric studies and one in remote sensing.
- *Cassini* will continue to explore Saturn's magnetosphere and its moons until 2017.
- ESA's first Small-class mission *CHEOPS (CHaracterizing ExOPlanets Satellite)* will look at exoplanets in detail. Its launch is expected in 2017.
- *Cluster*, ESA's four-spacecraft mission, is still providing unique data leading to a new understanding of space plasmas.
- The Chinese *ElectroMagnetic Satellite (EMS)* will be launched in 2016 to study the Earth's ionosphere.
- *InSight (INterior exploration using Seismic Investigations, Geodesy and Heat Transport)* is a NASA Discovery Program mission that will place a single geophysical lander on Mars to study its deep interior. It is expected for launch in 2016.
- ESA's *JUpiter ICy moons Explorer (JUICE)* will observe the giant gaseous planet Jupiter and three of its largest moons, Ganymede, Callisto, and Europa. It is planned for launch in 2022.
- *Juno* is a NASA mission dedicated to understand Jupiter's origin and evolution.
- *MMS* will use four identically equipped spacecraft to explore the acceleration processes that govern the dynamics of the Earth's magnetosphere. It is scheduled for launch in 2015.
- *Resonance* is a Russian space mission of four identical spacecraft, orbiting partially within the same magnetic flux tube, scheduled for launch in 2015.
- *Rosetta* is on its way to comet 67P/Churyumov-Gerasimenko. It will arrive in summer 2014 and deposit a lander in November.
- *Solar Orbiter* is to study along an innovative trajectory solar and heliospheric phenomena, planned for launch in 2017.
- *STEREO* studies solar (wind) structures with two spacecraft orbiting the Sun approximately at Earth's distance.

- *THEMIS* has been reduced to a near-Earth three-spacecraft mission. The two other spacecraft are now orbiting the moon in the *ARTEMIS* mission.
- The *Van Allen Probes* are two NASA spacecraft which quantify processes in the Earth's radiation belts.
- *Venus Express* explores the space plasma environment around Venus.

Two missions ended in 2013: The French space telescope *COROT* was decommissioned and ESA's Earth observer *GOCE* was deorbited in November.

IWF is naturally engaged in analyzing data from these and other space missions. This analysis is supported by theory, simulation, and laboratory experiments. Furthermore, at Lustbühel Observatory, one of the most accurate laser ranging stations of the world is operated.

## Highlights in 2013

- Oscillating magnetic fields in the Earth's magnetotail show their field-aligned current-driven signatures in the ionosphere and aurora.
- The calculated mass-loss of super-Earths shows that they cannot lose their hydrogen envelope and thus are more Neptune-like.
- Key instruments were delivered and mounted on the spacecraft of the upcoming missions *BepiColombo* and *Magnetospheric Multiscale*.

## The year 2013 in numbers

Members of the institute published 105 papers in refereed international journals, of which 34 were first author publications. During the same period, articles with authors from the institute were cited almost 3000 times in the international literature. In addition, 75 talks and 48 posters have been presented at international conferences by members of the IWF. Last but not least, institute members organized 13 sessions at international meetings.

## IWF structure and funding

IWF is, as a heritage since foundation, structured into three departments:

- Experimental Space Research
  (Head: Prof. Wolfgang Baumjohann)
- Extraterrestrial Physics
  (Head: Prof. Helmut O. Rucker)
- Satellite Geodesy
  (Head: Prof. Hans Sünkel)

Wolfgang Baumjohann serves as Director. All important decisions are discussed by an institute council consisting of the three research directors and six staff members. Scientifically, there are no walls between the three departments. Staff members from different departments work successfully together in six research fields (Fig. 1).

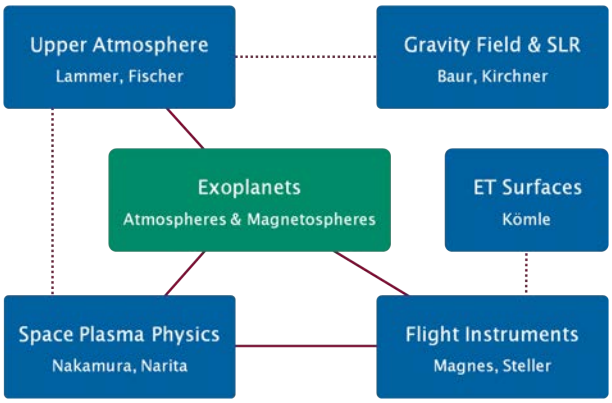


*Fig. 1: IWF research fields and group leaders.*

The bulk of financial support for the research is provided by the ÖAW. Substantial support is also provided by other national institutions, in particular the Austrian Research Promotion Agency (Österreichische Forschungsförderungsgesellschaft, FFG) and the Austrian Science Fund (Fonds zur Förderung der wissenschaftlichen Forschung, FWF). Furthermore, European institutions like ESA and the European Union contribute substantially.

# Earth & Moon

In the last decades, space geodesy has become an integral part in Earth and planetary sciences. Dedicated satellite missions provide high-quality data, which are nowadays indispensable for monitoring our home planet and to unlock secrets of the evolution of the Earth and the solar system. IWF analyzes these data with a special focus on the determination of the terrestrial and the lunar gravity field, selected studies of the Earth's atmosphere and crustal dynamics, as well as satellite laser ranging (SLR) to Earth-orbiting spacecraft and debris objects.

## Gravity Field

Knowledge about the gravity field is the key to unlock geophysical processes on the surface and in the interior of a body. Furthermore, due to the fact that satellite dynamics are dominated by the gravitational pulls acting on the spacecraft, the gravity field is of fundamental importance for orbit determination and mission design. At IWF, gravity field research activities include the analysis of data collected by the dedicated Earth-orbiting missions *GOCE* and *GRACE*, the lunar missions *LRO* and *GRAIL,* and SLR to passive satellites.

### GOCE

The core task of ESA's mission *GOCE (Gravity field and steady-state Ocean Circulation Explorer,* Fig. 2) is to provide data for the computation of a model of the Earth's static gravity field with unprecedented accuracy and resolution. The *GOCE* satellite was launched in spring 2009. The nominal mission duration was one year, but owing to less fuel consumption as initially expected, *GOCE* collected science data for about four years. Starting in August 2012 the orbit has been lowered in several steps from 255 km to 225 km. The end of mission was in November 2013, when *GOCE* reentered the Earth's atmosphere.

*Fig. 2: Artist's view of the GOCE satellite. Due to its aerodynamic design, the spacecraft is sometimes dubbed the "Ferrari of space" (Credits: ESA).*

***Data processing:*** IWF together with the Institute of Theoretical Geodesy and Satellite Geodesy of TU Graz form the *GOCE* team Graz, which processes the official *GOCE* time-wise (*GOCE*-TIM) gravity field solutions. This unit is part of the European *GOCE* Gravity Consortium, which consists of ten European institutions working under ESA contract.

***GOCE gravity field models:*** In March 2013, the fourth generation *GOCE* gravity field solutions have been released to the public by ESA. These models span almost three years of data, from November 2009 to July 2012 (opposed to twelve months of data used for the preceding third generation releases). Owing to the longer time span and huge effort put into the reprocessing of the science data, more small-scale features on and near the Earth's surface are now detectable from the space gravimetry measurements (Fig. 3). The fifth generaton releases, including the entire set of *GOCE* data, will be compiled in 2014.

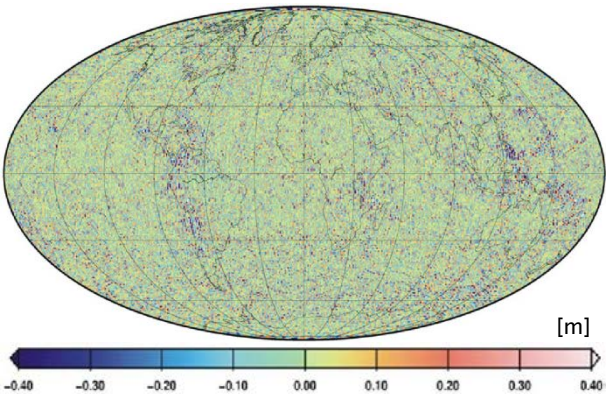


*Fig. 3: Differences between the fourth generation and the third generation GOCE geoid. The pattern reflects the noise reduction in the latest gravity field solution.*

***Orbit analysis:*** The *GOCE* mission provides a great opportunity to assess the performance of approaches that have been developed during the last decade to derive gravity field models from kinematic satellite orbits. This is of particular relevance against the background that in the absence of *GOCE* (decommissioned) and *GRACE* (likely to be decommissioned soon) kinematic orbit analysis will be the primary gravity field inference technique. Led by IWF, in a joint effort together with science institutions in Germany, Switzerland, The Netherlands, and Austria the following methods have been evaluated against each other:

- Energy balance approach
- Point-wise acceleration approach
- Averaged acceleration approach
- Short-arc approach
- Celestial mechanics approach

As major conclusion it turned out that apart from energy balance, the gravity field recovery approaches have compatible performance. This overall finding can be drawn if and only if a large degree of consistency in the data processing is provided. The energy balance approach, on the other hand, shows systematic shortcomings.

## GRACE

Since 2002, considerable effort is put in the computation of mass changes from time-variable *GRACE (Gravity Recovery And Climate Experiment)* gravity field solutions. The continuing mass loss of the Greenland ice sheets has gained particular interest, particularly against the background of the ongoing debate on global climate change. The remaining liftetime of the *GRACE* mission is hardly predictable, but it is very likely that a gap between *GRACE* and its successor *GRACE* follow-on (supposed to become operational in 2017 at the earliest) occurs.

This gap can be bridged with gravity field information obtained from *GNSS* (Global Navigation Satellite Systems) tracking of low-Earth orbiting satellites. The *Swarm* mission can be considered as the most promising bridging candidate. The spacecraft and orbit design is comparable to that of the *CHAMP (CHAlleng-ing Minisatellite Payload)* mission (operational from 2000 to 2010); as a consequence, time variability as seen by *CHAMP* provides evidence of space gravimetry based mass variation detection in the absence of *GRACE*.

The pattern shown in Fig. 4 suggests mass loss along the entire Greenland coastline and slight mass accumulation in the interior. The basin-wide *CHAMP* change rate is -246 ±10 Gt/yr. This value deviates by only 10% from the *GRACE* result (-223±10 Gt/yr).

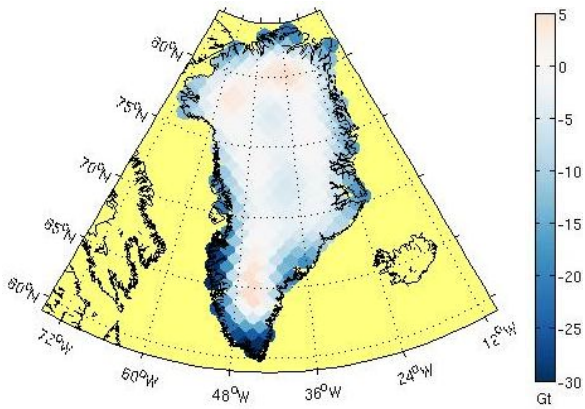


*Fig. 4: Greenland mass variation pattern from CHAMP time-variable gravity (2003-2009).*

## LRO

The NASA mission *Lunar Reconnaissance Orbiter (LRO)* was launched in 2009 to prepare

for save robotic returns to the Moon (Fig. 5). *LRO* is the first spacecraft in interplanetary space routinely tracked with 1-way optical laser ranges in addition to radiometric (Doppler shift) observations. As such, the mission provides a unique chance to investigate the capability of laser ranging for the determination of a satellite's orbit at a distance of roughly 400 000 km from Earth. The analysis of either laser ranges or Doppler data, as well as the combination of both, allows investigating the benefit of having two independent tracking data sets at hand.

*Fig. 5: Artist's rendering of the LRO spacecraft (Credits: NASA).*

First results indicate that *LRO* orbits estimated from laser ranges alone have a precision in total position of about 100 m. The main reason for this rather large value can be traced back to the sparse laser tracking data, on the one hand, and the involvement of two non-synchronous clocks, on the other hand. When using 2-way Doppler measurements, which are continuously available, the precision increases considerably to about 15 m in total position.

In a next step, the two measurement types will be analyzed in a joint parameter estimation procedure. The resulting "best" *LRO* orbit will constitute the basis for the recovery of the long-wavelength lunar gravity field. The lack of tracking data over the farside of the Moon will require regularization to stabilize the normal equation systems.

## GRAIL

The *Gravity Recovery And Interior Laboratory (GRAIL)* twin-satellite mission orbited the Moon from March to December 2012. *GRAIL* is the first dedicated gravity mission in planetary science; the mission concept (Fig. 6) is inherited from the *GRACE* project. Prior to *GRAIL*, lunar gravity field determination was limited due to the lack of measurements on the farside (1:1 Earth-Moon spin-orbit resonance) and due to the accuracy of ground-based Doppler orbit tracking data. Owing to high-precision inter-satellite observations with global coverage, the *GRAIL* mission allows to infer the lunar gravity field with unprecedented accuracy and spatial resolution. Accordingly, *GRAIL* is supposed to considerably improve our knowledge about the interior structure and thermal evolution of the Moon.

At IWF, *GRAIL* data analysis is performed in cooperation with the Institute of Theoretical Geodesy and Satellite Geodesy at TU Graz, making use of a novel inference technique in planetary sciences. The inter-satellite ranging data is exploited by an integral equation approach using short orbital arcs; it is based on the reformulation of Newton's equation of motion as a boundary value problem. The integral equation approach is an alternative to more commonly applied gravity field recovery methods based on variational equations.

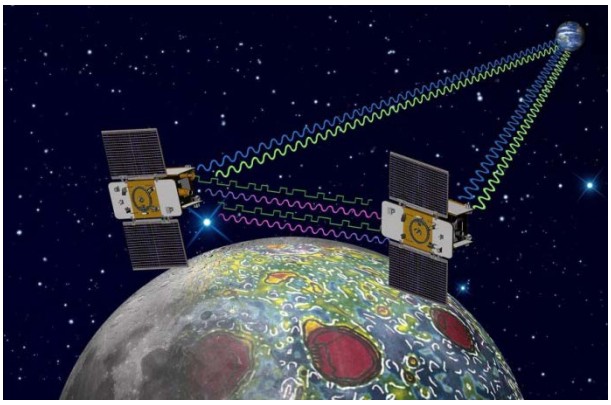

*Fig. 6: GRAIL mission design. The two satellites are following each other in the same orbit. Each spacecraft is tracked from stations on the Earth via radio signals; the relative motion between the spacecraft is observed by an inter-satellite link (Credits: NASA).*

# Geodynamics

*Plate observations:* The relative motion of tectonic plates is the major source of earthquakes. The strongest quakes occur at plate boundaries; therefore, knowledge about the localization and temporal variation of these boundaries is of utmost relevance. The most important boundary zone in Europe is the collision zone near Greece, where the Eurasian Plate and the Nubian Plate meet each other, creating several minor plates and a multitude of plate boundaries. Global Navigation Satellite System *(GNSS)* time series can help to model the velocities and delineations of these plates, and hence contribute to the better understanding of their movements. In 2013, a new permanent *GNSS* network (called GREECE) has been created from about 170 (90 of them are presently active) freely available stations operating from 2006–2013.

# Atmosphere

*Atmospheric density response to flares:* Investigations on the impact of flares on the mass density in the Earth's upper thermosphere were performed. The main aim is to use flares and Coronal Mass Ejections (CMEs) as proxies for young Sun atmosphere response studies. A prerequisite for this procedure is the appearance of isolated solar flares. Upper atmosphere density enhancements exclusively caused by an isolated flare are not very numerous – often they are accompanied by CMEs. Additionally, dealing with *GRACE* accelerometer data requires the events to be "visible" for the satellite in terms of spacecraft position.

Another difficulty is that events often appear within short periods. Thus, the assignment of density enhancements to flares may be ambiguous, because knowledge about the time delay between the appearance of the enhanced X-ray flux at the Earth and the density enhancement is still sparse. Against this background, investigations are targeting an improved understanding of the phenomena associated with flares and CMEs. CME-induced events, e.g., appear mainly in the polar regions (Fig. 7), whereas flares can enhance density at the whole dayside.

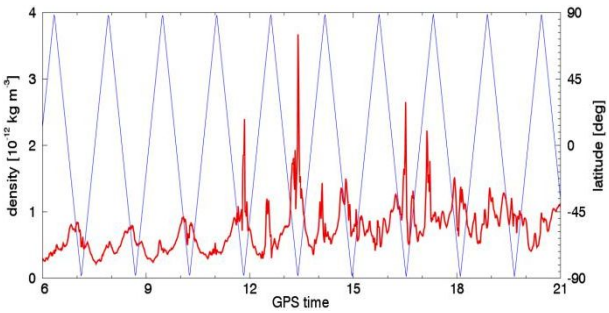


*Fig. 7: GRACE-A on 17 January 2005. Blue graph: geocentric latitude. Red graph: density enhancements; the four peaks between 11:45 h and 17:30 h are seen in the polar regions, as it is typical for CME events.*

*Multipath:* Apart from the Earth's ionosphere, multipath is still the dominant error source for many *GNSS* applications. Especially multipath effects caused by reflectors in the vicinity of the receiver antenna are to date hard to mitigate or compensate. The core idea of the realized concept is to generate a synthetic aperture from the displacement of the antenna element. Two antennas – one rotating and one vertically moving – were manufactured and tested (Fig. 8). These antennas are designed to reduce multipath effects to a harmless level.

*Fig. 8: Rotating antenna at the roof of the IWF building. An artificial reflector realized by a copper plate was installed to generate multipath effects in addition to these ones caused by the "natural" environment.*

# Satellite Laser Ranging

Besides the routine tracking of satellites equipped with retro-reflectors (in the framework of the activities of the International Laser Ranging Service, ILRS), the experimental tracking of space debris targets continued. In addition, in 2013 orbit determination and orbit prediction of debris objects was started. Further SLR activities include bi-/multi-static experiments and satellite spin detection.

***Space debris tracking:*** A laser from DLR (Deutsches Zentrum für Luft- und Raumfahrt) used during the last year (1 kHz, 20 mJ/shot) was replaced by another laser borrowed from DLR with (almost) 100 Hz repetition rate and 200 mJ/shot. New detection hardware – using a 500 µm diameter Peltier-cooled avalanche diode – was developed and installed. These new detection packages yielded an increase in efficiency and the reduction of dark noise, and they allow for easier tracking of targets with very low-accuracy predictions. The results demonstrate the capability to range to debris targets as small as 0.3 $m^2$, and to larger targets up to distances of 3100 km. During eleven space debris ranging sessions, about 140 passes of debris targets have been tracked successfully.

***Precise orbit determination:*** The reliable and accurate orbit determination and orbit prediction of debris objects is of crucial importance for any effort towards Space Situational Awareness. However, the sparseness and poor quality of available observations (Fig. 9), missing attitude information of the objects with respect to inertial space, and the lack of retro-reflectors make trajectory determination/prediction a highly challenging task. By means of tailored processing in order to cope with these "harsh conditions", very good results for the defunct ENVISAT satellite were achieved. The *ENVISAT* orbit predictions computed at IWF are officially distributed via the ILRS website.

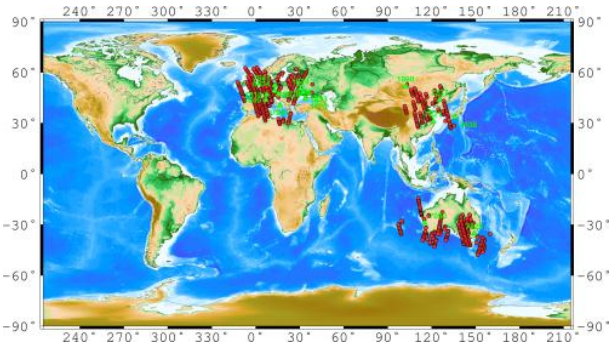


*Fig. 9: Spatial distribution of SLR observations to the defunct ENVISAT satellite in September 2013 (in red).*

***Multi-static experiments:*** In addition to previous bi-static measurements, the first multi-static experiments were successful: the SLR stations in Zimmerwald (Swiss), Wettzell (Germany) and Herstmonceux (UK) were able to detect photons emitted in Graz, diffusely reflected from debris targets (Fig. 10). Owing to the unique concentration of SLR stations in Europe, such multi-static observations to space debris targets will allow for more accurate orbit determination compared to stand-alone "traditional" ranging.

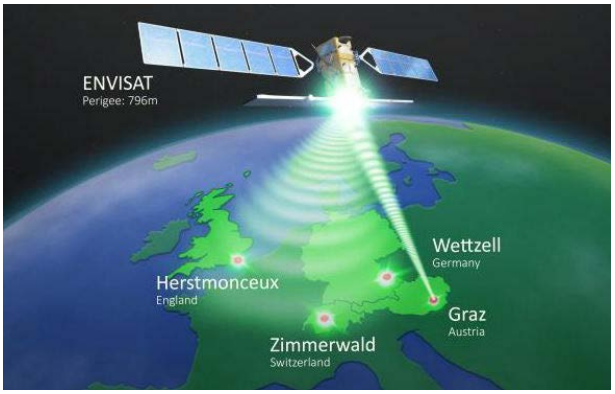


*Fig. 10: Multi-static experiment: the passive SLR stations in Wettzell, Zimmerwald and Herstmonceux were able to receive photons emitted in Graz (Credits: AIUB).*

***Satellite spin detection:*** Since April 2012, the *ENVISAT* satellite is defunct, and hence has to be considered as a space debris object. The 8-tons satellite speeds along a crowded sun-synchronous orbit in an altitude of about 800 km. Due to the lack of any control the satellite slowly changed its attitude, and finally started to spin. Since it is difficult to obtain information about this attitude and the spin parameters, IWF started a campaign within the

ILRS to range again to *ENVISAT*, using its retro-reflectors whenever they are visible from ground stations. Based on this SLR data it could be shown that the *ENVISAT* satellite (i) has obtained a stable orientation, fixed with respect to its orbit, (ii) spins with an inertial period of 134.74 s (value from 25 September 2013), and (iii) that the spin period increases by 36.7 ms per day. The satellite spins in counter-clockwise direction; the solar array approaches the along track and the radial vectors consecutively (Fig. 11).

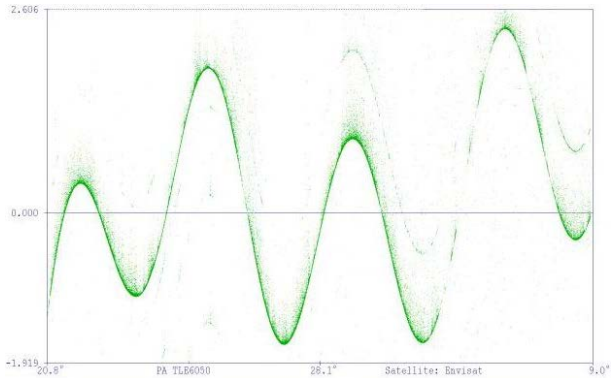


*Fig. 11: ENVISAT spin as detected by SLR. Shown is the large-scale motion of the retro panel (±2 m).*

***Quantum cryptography:*** Within a cooperation between IWF and the Institute for Quantum Optics and Quantum Information (IQOQI) a completely new detection section of the SLR telescope was designed and started to be built. The planned transmission of quantum cryptography keys via satellite needs several additional single-photon detector packages and has to handle new wavelengths (1064 nm, 810 nm, 710 nm). While the old detection package allows for a maximum of two different detectors (with difficult installation and alignment procedures) the new one is designed for up to four detection channels (plus four channels for the quantum experiment), supported by several CCD cameras.

***Nano-satellite tracking:*** An initiative was started to equip nano-satellites in low-Earth orbits with one or several retro-reflectors; this will allow precise orbit determination not only during the operational phase, but also beyond the active mission lifetime – such as in case of technical failures. It could be shown that for orbits around 600 km altitude or lower it is sufficient to use single, off-the-shelf, cheap corner cubes of 10-12 mm diameter, without special shapes or dihedral angles to compensate for velocity aberration (Fig. 12).

In addition, multiple retro-reflectors on each side of these small (and light) satellites will allow attitude determination with an accuracy of better than 1°. At present, four nano-satellites are foreseen to be equipped with retro-reflectors: OPS-SAT (ESA), TechnoSat (TU Berlin), S-Net (TU Berlin), and CubETH (ETH Zürich). The launches of these satellites are planned in 2015-2016.

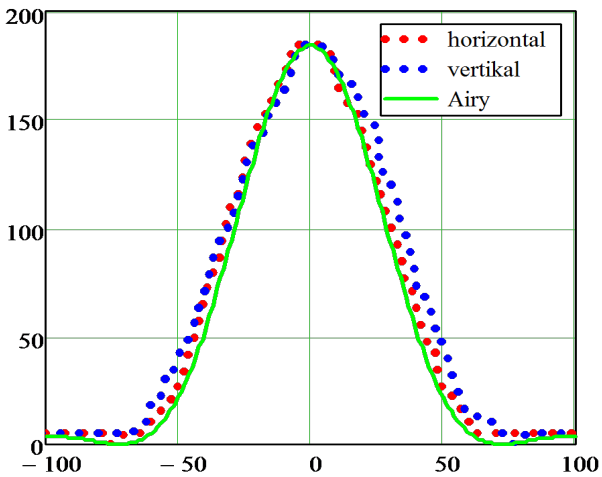


*Fig. 12: Off-the-shelf retro-reflector performance. Calculated radar cross section at an orbital altitude of 600 km.*

# Near-Earth Space

Near-Earth space is an ideal natural laboratory to study space plasmas physics with in-situ measurements of the charged particles together with electric and magnetic fields. IWF both builds instruments for satellite missions that make measurements in this natural laboratory and analyzes the data obtained by them, and participates in future planning.

## Missions

The *Cluster* and *THEMIS/ARTEMIS* missions are providing a wealth of exciting data, which lead to many new scientific results. Furthermore, IWF is involved in the upcoming *MMS* mission.

### Cluster

The four *Cluster* spacecraft, launched in 2000, study small-scale structures of the magnetosphere and its environment in three dimensions. The spacecraft are taking data while circling the Earth in polar orbits. The separation distance of the spacecraft has been varied between 200 km and 10 000 km according to the key scientific regions. This ESA mission has been extended to December 2016. IWF is PI of the spacecraft potential control and holds Co-I status on four more instruments.

### THEMIS/ARTEMIS

NASA's *THEMIS* mission, launched in 2007, is designed to explore the origin of magnetic storms and auroral phenomena. *THEMIS* flies five identical satellites through different regions of the magnetosphere. As Co-I institution of the magnetometer, IWF is participating in processing and analyzing data. The two outer spacecraft became a new mission, *ARTEMIS*, to study the Moon, the distant magnetotail, and the solar wind from autumn 2010. The other three *THEMIS* spacecraft remained in their orbit to further study the dynamics of the inner magnetosphere.

### Van Allen Probes

The *Van Allen Probes* (formerly known as the *Radiation Belt Storm Probes)*, successfully launched in 2012, are studying the dynamics of the radiation belts essential for understanding the key component of the space weather system. The instruments on the two *Van Allen Probes* spacecraft provide the measurements needed to characterize and quantify the processes that produce relativistic ions and electrons. As one of the science Co-I institutes, IWF analyzes the data combined with other magnetospheric missions and ground-based data.

### MMS

NASA's *MMS* mission *(Magnetospheric Multi-scale)* will explore the dynamics of the Earth's magnetosphere and its underlying energy transfer processes. Four identically equipped spacecraft are to carry out three-dimensional measurements in the Earth's magnetosphere. *MMS* will determine the small-scale basic plasma processes, which transport, accelerate and energize plasmas in thin boundary and current layers. *MMS* is scheduled for launch in 2015. IWF has taken the lead for the spacecraft potential control of the satellites *(ASPOC)* and is participating in the electron beam instrument *(EDI)* and the digital fluxgate magnetometer *(DFG),* which both are part of the *FIELDS* instrument package (Fig. 13).

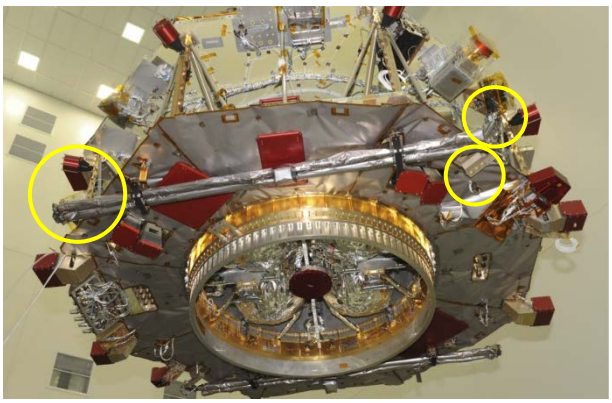

*Fig. 13: Spacecraft 1 lifted up in the MMS clean room at NASA's Goddard Space Flight Center (GSFC); EDI (left), ASPOC (upper right) and the DFG sensor on the magnetometer boom (lower right) are marked by yellow circles (Credits: SwRI/Ron Black).*

***Active Spacecraft Potential Control (ASPOC) instrument:*** End of February 2013, the last two (out of eight) Flight Models were delivered to the US. All models saw a complete sequence of integration of electronics with ion emitter modules, comprehensive performance testing, vibration, thermal vacuum, EMC, and magnetic tests. Before delivery of the units in pairs to the US, their data packages were compiled and reviewed. Environmental testing was uneventful with the exception of minor issues related to the ion emitters, which required partial re-testing of two Flight Models. Reporting, scheduling, and maintenance of data bases were done as necessary.

After integration of the Flight Models into the Instrument Suites and Observatories at GSFC, a series of observatory level tests including EMC, shock, acoustics, thermal balance and thermal vacuum test has started. On the software side, several improvements to the onboard software concerning the emitter operation have been implemented and tested. After performing the formal acceptance test, the software will be installed on all Flight Models once the environmental testing of the observatories has finished (June 2014). The preparations for system tests and the in-flight commissioning in 2015 were ongoing and the development of the Science Data Processing software has started.

***Electron Drift Instrument (EDI):*** IWF contributes to *EDI* with the *Gun Detector Electronics (GDE)* and the electron gun. The *GDE* is developed by Austrian industry in close cooperation with the institute, while the electron gun is entirely developed by IWF.

The *EDI* instrument for *MMS* is based on the *Cluster* development with several improvements. In 2013 IWF manufactured, calibrated and delivered the flight units FM4 to FM7. The contribution of the industry is completed and all nine *GDE* flight models are either available or delivered.

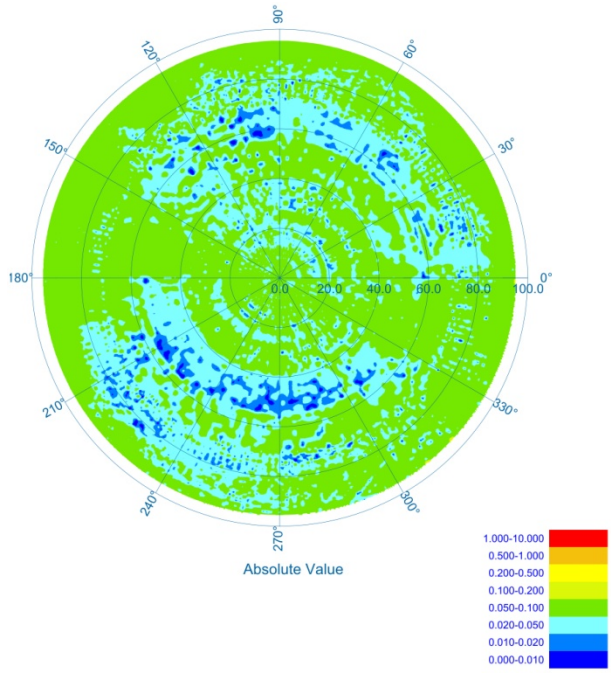


*Fig. 14: Pointing accuracy, typically better than 0.1°.*

The calibration process is an important step to get an accurate pointing of the electron gun. The requirement is to emit the electron beam with a pointing accuracy of 1° within the 2π sr. On average, the achieved accuracy is much better. The calibration process is done in 2° steps in polar and azimuthal angle. For polar angles above 70° the stepsize for azimuth is 1°. This results in 21600 reference points to generate the correction table. Fig. 14 shows the perfect results for FM7 at the 1 keV energy level. FM8 is presently manufactured and will be delivered together with the last model (FM9) in early 2014.

*Digital Flux Gate magnetometer (DFG):* *DFG* is based on a triaxial fluxgate developed by the University of California, Los Angeles, and a front-end Application Specific Integrated Circuit (ASIC) for magnetic field sensors. The ASIC has been developed by IWF in cooperation with the Fraunhofer Institute for Integrated Circuits in order to reduce the size, mass and power consumption of the near sensor electronics. In 2013, the spare model of DFG was assembled and calibrated at IWF. Parallel to the final hardware assembly activities, IWF supported the spacecraft integration of the flight magnetometers with all related functional tests.

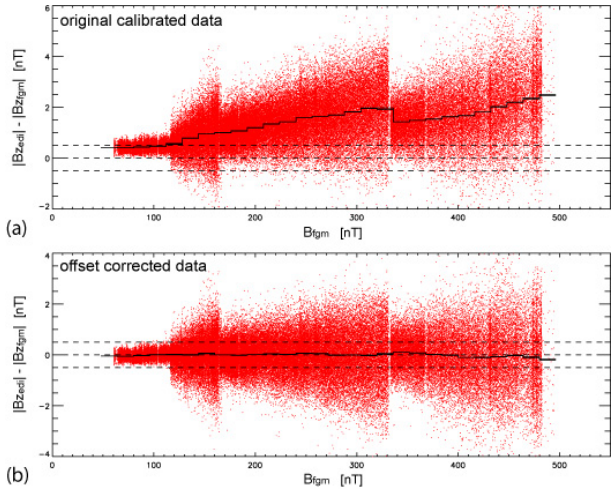


*Fig. 15: Difference between spin axis component EDI and FGM fields for (a) the original calibrated data and (b) offset calibrated data.*

*Cross Calibration:* New methods of determining spin axis offset of the flux magnetometers *(FGM)* using absolute magnetic field values deduced from the time of flight data from the *EDI* measurements have been investigated to be included as part of the in-flight magnetometer calibration for *MMS*. Using *Cluster* data, it is demonstrated that the method works when the effects of the different measurement conditions, such as direction of the magnetic field relative to the spin plane and field magnitude, as well as the time-of-flight offset of the *EDI* measurements are properly taken into account (see Fig. 15).

## EMS

The *Electro-Magnetic Satellite (EMS)* mission is scheduled for launch end of 2016 and will be the first Chinese platform for the investigation of natural electromagnetic phenomena with major emphasis on earthquake monitoring from a polar Low Earth Orbit (LEO).

The *EMS* magnetometer is developed in cooperation between the Center for Space Sciences and Applied Research (CSSAR) of the Chinese Academy of Sciences, IWF and the Institute of Experimental Physics of the Graz University of Technology (TUG). CSSAR is responsible for the dual sensor fluxgate magnetometer, the instrument processor and the power supply unit, while IWF and TUG participate with the newly developed absolute scalar magnetometer called *CDSM*. In 2013, the *CDSM* Engineering Model was manufactured and tested. It is scheduled for delivery to China end of February 2014.

## Space Weather Magnetometer

The *Magnetometer Front-end ASIC (MFA)* developed by IWF, together with *Anisotropic Magneto-Resistive (AMR)* sensors, is in use for the development of a service oriented magnetometer package for space weather measurements. It is a flexible design with up to six magnetic field sensors. The *MFA-AMR* combination is used for detecting and characterizing magnetic disturbers of the spacecraft body so that the data measured by the fluxgate sensor at the tip of an up to 2 m long boom (also part of the package) can be corrected for the spacecraft magnetic fields. It is planned to fly such magnetometers on missions, which are not necessarily dedicated to scientific objectives but which go to orbits where space weather forecast measurements are useful. In 2013, an ESA-funded first prototype of the *MFA-AMR* magnetometer was developed.

# Physics

Various data from ongoing missions are analyzed and theoretical models are developed to describe the physical processes responsible for the formation of structures and phenomena in the Sun-Earth system at different scales. Most of the data analysis is performed using data provided by the ongoing *Cluster* and *THEMIS* missions, as well as other magnetospheric missions and ground-based observations. The studies deal with interactions between solar wind and magnetosphere, internal disturbances in the magnetosphere such as plasma flows and waves, and plasma instabilities including magnetic reconnection.

***Current sheet thickness in the Earth's magnetotail:*** A new mathematical tool has been developed to unambiguously and directly estimate the current sheet thickness in the Earth's magnetotail. The technique is a combination of eigenvalue analysis and minimum variance estimation adapted to a Harris current sheet geometry, and needs simultaneous four-point magnetic field data as provided by the *Cluster* spacecraft. Two current sheet parameters, thickness and distance to the spacecraft, can be determined any time.

The method was applied to an interval of *Cluster* magnetotail crossings in 2006 under quiet magnetospheric conditions, and the current sheet thickness was estimated to be on the scale of the local proton gyroradius (of the order of several thousand km). Fig. 16 displays the histogram of the current sheet thickness in units of the local proton gyroradius. The thickness is distributed from the proton gyroradius (or smaller) up to 20 gyroradii. The histogram fits reasonably a combination of Gaussian distributions, centered at about 1.4, 3.1, and 9.3 gyroradii. Large variation in the thickness distribution agrees with the earlier estimates using different methods, and supports the notion of multi-scale or embedded current sheet structures. The analysis technique can be used to track the dynamical evolution of the current sheet structure in the magnetotail.

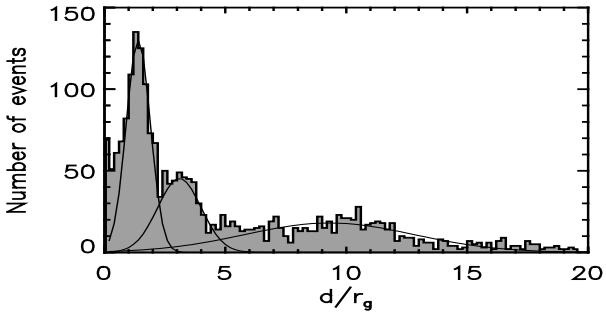


*Fig. 16: Histogram of determined current sheet thickness d normalized to gyroradius of thermal protons. Dashed lines show fittings with multiple Gaussian distributions.*

***Magnetic field topology of the plasma sheet boundary layer (PSBL):*** The PSBL is situated between the magnetotail lobe and the central plasma sheet, a region that is thought to be primarily responsible for mass and energy transport between the magnetosphere and the high-latitude ionosphere during disturbed geomagnetic conditions. The 3D magnetic field topology of the PSBL is shown for the first time (Fig. 17), using the reconstruction method, which is an analysis method that applies single spacecraft data to MHD force balance equations in order to recover the surrounding spatial structures of plasma and fields measured by the *Cluster* spacecraft during the substorm recovery phase.

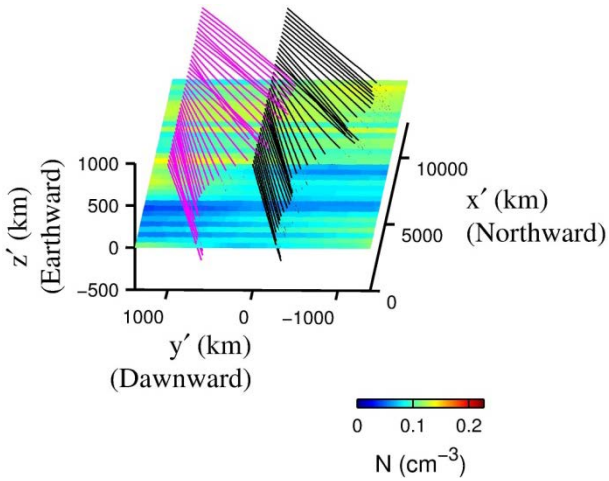


*Fig. 17: 3-D illustration of the reconstructed PSBL with the plasma density in color.*

In Fig. 17, the black and magenta magnetic field lines are oriented tailward, starting at

Z'=1000 km along the line Y'=0 km and 1000 km, respectively. The figure reveals that the field lines are being perturbed along the dawn-dusk direction, resulting in a wavy magnetic structure for the PSBL. In addition, the wavy PSBL structure is found to have significant electric currents along the magnetic field lines. These field-aligned currents can be well estimated by the reconstruction method.

***Anti-sunward high-speed jets in the subsolar magnetosheath:*** Using four years data of NASA's five-spacecraft *THEMIS* mission, the properties and favorable solar wind conditions for the occurrence of high-speed jets in Earth's subsolar magnetosheath were studied. High speed jets occur downstream of the quasi-parallel bow shock, i.e., when the interplanetary magnetic field is essentially directed along the Earth-Sun-line. Jet occurrence is only very weakly dependent on other upstream conditions or solar wind variability.

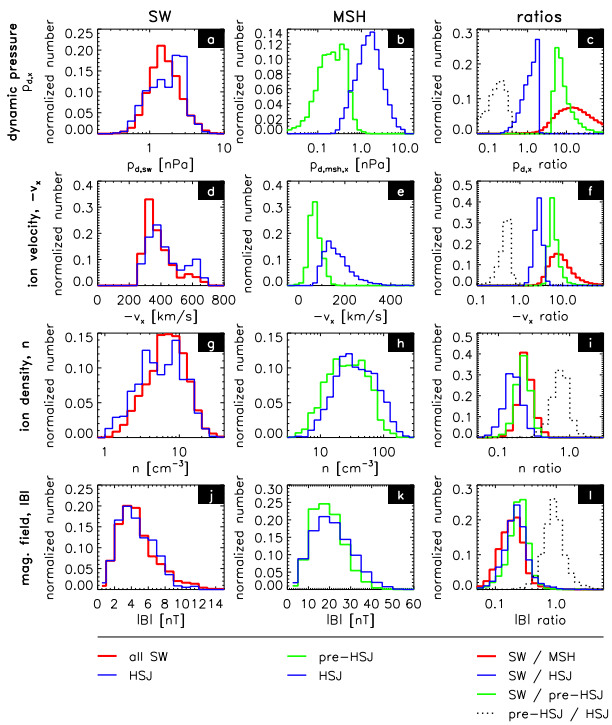


*Fig. 18: Distributions of solar wind (SW) and magnetosheath (MSH) ion dynamic pressure, velocity, density, and magnetic field observations in general, as well as before and during high-speed jets (HSJ).*

Relative to the ambient magnetosheath, high-speed jets exhibit much higher plasma speed, somewhat higher density and magnetic field intensity (see Fig. 18), but lower and more isotropic temperatures. The jets are almost always super-Alfvénic, often even super-magnetosonic, and typically feature twice as high total pressure toward the magnetopause as the surrounding plasma does. Consequently, high-speed jets are likely to have a significant impact on the magnetosphere and ionosphere if they hit the magnetopause.

***Azimuthal size of flux ropes near lunar orbit:*** Magnetic flux ropes are formed during magnetic reconnection in the Earth's magnetotail and serve as transporter of magnetic flux, energy and accelerated plasma during the course of substorms. Previous observations of flux ropes in the mid- and distant tail were restricted to single spacecraft observations. Hence, an accurate determination of spatial scales of these 3D structures is difficult. With *ARTEMIS*, two probes cross the magnetotail near lunar orbit for ~4 days every lunar month and allow two-point flux rope observations.

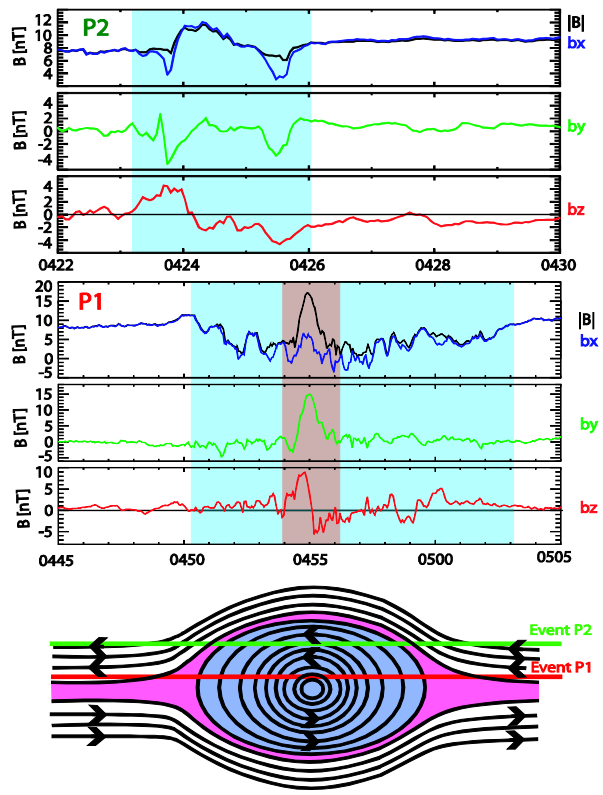


*Fig. 19: Magnetic field observations made by ARTEMIS probes P2 (top) and P1 (middle) during two flux rope encounters. The different behavior of the magnetic field indicates different paths of the probes through the flux ropes (bottom).*

*ARTEMIS* observations (Fig. 19) show that the typical dawn-dusk flux rope extent is ~6 RE and hence smaller than previously thought. For high geomagnetic activity levels flux ropes with azimuthal size >9 RE are common. Flux rope crossings at different distances to their axis also reveal their internal structure.

***Transient electron precipitation during oscillatory BBF braking:*** Using *THEMIS* data acquired on 17 March 2008 between 10:22 and 10:32 UT (Fig. 20) the mechanism of transient electron injection into the loss cone during oscillatory bursty bulk flow (BBF) braking is studied. During braking, transient regions of piled-up magnetic fluxes are formed. Perpendicular electron anisotropy observed in these regions may be a free-energy source for co-existing whistler waves. Parallel electrons with energies of 1-5 keV disappear inside these regions and transient auroral forms are observed simultaneously by the all-sky imager at Fort Yukon. Quasi-linear diffusion coefficients during electron resonant interaction with whistler waves are estimated. It is found that electron injection into the loss cone is caused by whistler waves scattering.

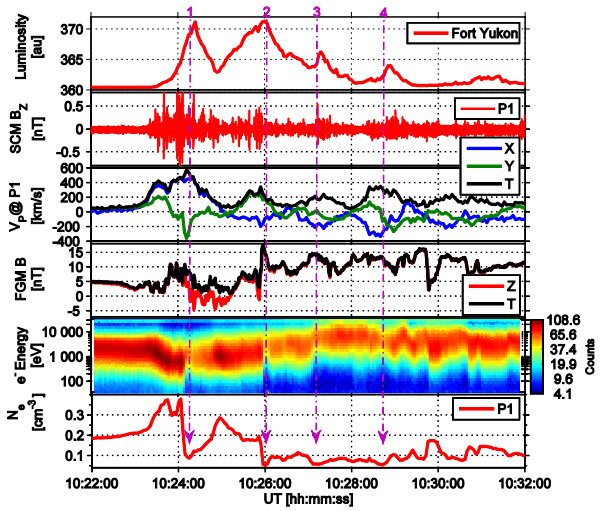


*Fig. 20: THEMIS data on 17 March 2008 between 10:22:00 and 10:32:00 UT: (a) total luminosity observed by the all-sky imager at Fort Yukon, (b) Z-component of the magnetic field oscillations from search-coil magnetometer (SCM), (c) X-, Y-, and total component of the ion velocity from ESA, (d) Z-, and total component of the magnetic field from fluxgate magnetometer (FGM), (e) electron energy spectrogram, and (f) electron density from ESA at P1.*

***Dipolarization front and flow bouncing:*** One of the unsolved problems in the Earth's magnetotail physics is the dissipation process of the Earthward transported energy via fast plasma flows. Interaction between the fast Earthward plasma flows accompanied by sharp magnetic field front structure, called the dipolarization front, and the ambient plasma in the near-Earth nightside magnetosphere is studied based on *Cluster* multipoint observations. A series of dipolarization fronts were detected starting with a localized (<2 RE) dipolarization front and ending with a large scale (>10 RE) and stronger dipolarization front immediately followed by flow bouncing, i.e. reversal of the flow direction (Fig. 21). The stronger electric field and substantial changes in particle energy suggest that the major energy conversion takes place in the near-Earth flow bouncing region rather than during the Earthward propagation of the dipolarization front. Although the overall enhanced energetic electron flux seems to be dependent on the spatial scale of the front and the strength of the dawn-to dusk electric field, it is shown that a major energization event can take place locally or temporal in the near-Earth region.

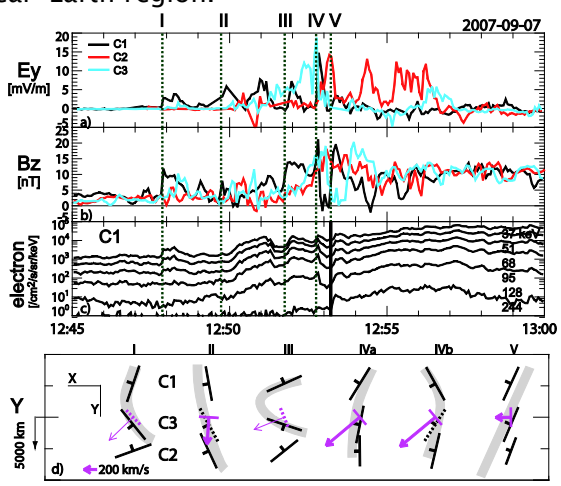


*Fig. 21: Cluster (C1, C2, C3) observations of dipolarization fronts (I-V). (a) EY (dawn-to-dusk electric field), (b) BZ (magnetic field component showing dipolarization), and (c) differential flux of high-energy electrons from C1 and (d) the orientation of the dipolarization fronts in the X-Y (equatorial) plane. The arrows show the propagation of the dipolarization front determined from multipoint observations.*

# Solar System

IWF is engaged in many space missions, experiments and corresponding data analysis addressing solar system phenomena. The physics of the Sun and the solar wind, its interaction with solar system bodies and various kinds of planetary atmospheres and surfaces are under investigation.

## Sun & Solar Wind

The Sun's electromagnetic radiation, magnetic activity, and the solar wind are strong drivers for various processes in the solar system.

### Solar Orbiter

*Solar Orbiter* is a future ESA space mission to investigate the Sun, scheduled for launch in 2017. Flying a novel trajectory, with partial Sun-spacecraft corotation, the mission plans to investigate in-situ plasma properties of the near solar heliosphere and to observe the Sun's magnetized atmosphere and polar regions. IWF builds the digital processing unit (DPU) for the *Radio and Plasma Waves (RPW)* instrument onboard *Solar Orbiter* and has calibrated the *RPW* antennas, using numerical analysis and anechoic chamber measurements. Furthermore, the institute contributes to the magnetometer.

***Radio and Plasma Waves (RPW):*** *RPW* will measure the magnetic and electric fields at high time resolution and will determine the characteristics of the magnetic and electrostatic waves in the solar wind from almost DC to 20 MHz. Besides the 5-m long antennas and the AC magnetic field sensors, the instrument consists of four analyzers, the thermal noise and high frequency receiver, the time domain sampler, the low frequency receiver, and the bias unit for the antennas. The control of all analyzers and the communication with the spacecraft will be performed by the DPU.

The institute is responsible for the design of the DPU hardware and the boot software. In the first quarter of 2013 the prototype board has been delivered to LESIA to be used as reference model for the flight software development. The two engineering models, a fully flight representative model, but on lower components quality level, has been delivered in the third quarter. Presently, minor redesign and -layout is under preparation, implementing the "lessons learned" from the engineering model. A first release of the boot software has been delivered too. The next development step, the qualification model with the final boot software, will keep the team busy until mid 2014.

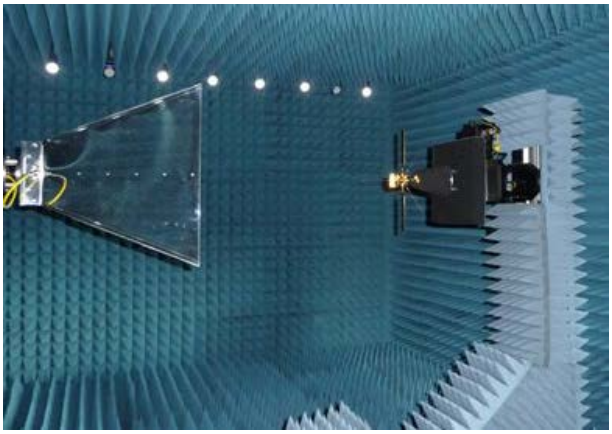

*Fig. 22: A scale model of the Solar Orbiter spacecraft placed in an anechoic chamber for antenna calibration measurements.*

The E-field sensors (boom antennas) of the *RPW* instrument aboard the *Solar Orbiter* spacecraft are subject to severe influences of

the conducting spacecraft body. Different methods were employed to find the true antenna properties. In an effort to complement numerical simulations, a 1:50 scale model of the spacecraft has been built and tested in an anechoic chamber as depicted in Fig. 22.

Direct comparisons between numerical simulation and measurement have been made, providing an important benchmark for the numerical results. The top two radiation patterns in Fig. 23 show a reasonable agreement between the anechoic chamber measurements (left) and FEKO numerical simulations (right). In the anechoic chamber, the co- and crosspolar patterns have also been measured (c.f. Fig. 23 bottom), which provide useful input to goniopolarimetry techniques like polarization analysis, direction finding and ray tracing.

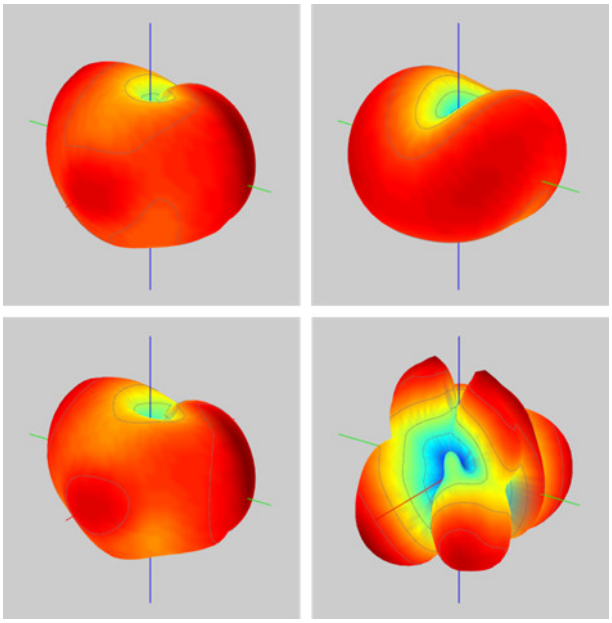

*Fig. 23: Directivity patterns for Solar Orbiter scale model at 600 MHz (scales down to 600/50=12 MHz). Top: anechoic chamber measurement (left) compared to FEKO simulation (right). Bottom: copolar (left) and crosspolar (right) anechoic chamber measurements.*

## Physics

***Radio seismology of the outer solar corona:*** Energetic electron beams generated during solar flares excite Langmuir oscillations in coronal loops, which emit radio emission at corresponding frequencies as type IV bursts. Global oscillations of coronal loops excited by the same flare modify the electron beam density, which may influence the amplitude of Langmuir oscillations and consequently the intensity of radio emission. Therefore, long period modulations of radio emission intensity could be caused by coronal loop oscillations. Comparison of observed periodicities with the theoretical spectrum of coronal loop oscillations allows estimation of the plasma parameters in the coronal loops.

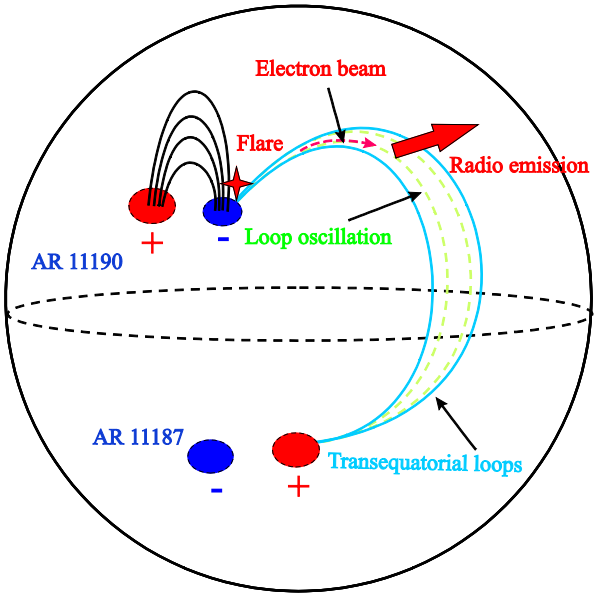


*Fig. 24: Schematic picture of radio emission from a transequatorial coronal loop after C2.3 solar flare on 14 April 2011.*

The large Ukrainian radio telescope URAN-2 observed type IV radio burst in the frequency range of 8-32 MHz during the time interval of 09:50-12:30 UT on 14 April 2011. The burst was connected to a C2.3 flare, which occurred in the active region AR 11190 during 09:38-09:49 UT. Wavelet analysis at four different frequencies (29 MHz, 25 MHz, 22 MHz, and 14 MHz) shows the quasi-periodic variation of emission intensity with periods of 34 min and 23 min. The periodicity can be explained by the first and second harmonics of transequatorial coronal loop oscillations (Fig. 24). The apex of transequatorial loops may reach up to 1.2 $R_S$, where $R_S$ is the solar radius, therefore the estimation of plasma parameters

at these heights is possible. The seismologically estimated Alfvén speed at 1 $R_S$ is ~1000 km $s^{-1}$. Consequently, the magnetic field strength at this height is estimated as ~0.9 G. Extrapolation of magnetic field strength to the inner corona gives ~10 G at the height of 0.1 $R_S$. Radio observations can be successfully used for the sounding of the outer solar corona, where EUV observations of coronal loops fail because of rapid decrease in line intensity.

*Doppler effect in solar wind turbulence:* A theoretical model of the energy spectrum for solar wind turbulence has been constructed by incorporating the effects of Doppler shift and broadening. In this model the solar wind magnetic field data measured by the four *Cluster* spacecraft (Fig. 25) were analyzed. This is the very first study of detailed spatio-temporal dynamics in solar wind turbulence using *Cluster* data and the high-resolution spectral analysis "Multi-point Signal Resonator".

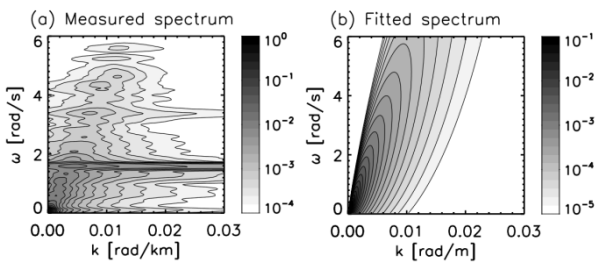


*Fig. 25: Panel (a): Energy spectrum derived from magnetic field data of Cluster, using the high-resolution wave number analysis technique. Panel (b): Reconstruction of the turbulence spectrum using the Doppler-shift-and-broadening model.*

The measured Doppler shift was consistent with that expected from the ion bulk speed, while the measured Doppler broadening was not small as expected from the amplitude of the fluctuations in the ion bulk speed but much larger. The discrepancy in the Doppler broadening indicates that solar wind turbulence does not represent only anti-sunward propagating waves, but also counter-propagating waves toward the Sun. The large Doppler broadening also implies that Taylor's frozen-in flow hypothesis, time series are purely convected spatial structures, is invalid for solar wind turbulence.

# Mercury

Mercury is now in the center of attention because of the current NASA *Messenger* mission and the upcoming ESA/JAXA *BepiColombo* mission. The planet has a weak intrinsic magnetic field and a mini-magnetosphere, which strongly interacts with the solar wind.

## BepiColombo

Two spacecraft, to be launched in 2016, will simultaneously explore Mercury and its environment: the Japanese *Magnetospheric (MMO)* and ESA's *Planetary Orbiter (MPO)*. IWF plays a major role in developing the magnetometers for this mission: it is leading the magnetometer investigation aboard the *MMO (MERMAG-M)* and is responsible for the overall technical management of the *MPO* magnetometer *(MERMAG-P)*. For *MPO*, IWF also leads the development of *PICAM,* an ion mass spectrometer with imaging capability, which is part of the *SERENA* instrument suite, to explore the composition, structure, and dynamics of the exo/ionosphere.

*Fig. 26: A MERMAG-P Flight Model with electronics box (center), two fluxgate sensors (front right and left) and two thermal protection covers for the fluxgate sensors with highly reflective mirrors (background right and left).*

In the first half of 2013, the instrument level testing of the *MERMAG-P* Flight Model (Fig. 26) was finished. In July 2013 it was delivered

to Turin for integration on the *MPO* spacecraft. The *MERMAG-M* Flight Model (FM) electronics and sensor, which were delivered to Japan in 2012, were mounted on the *MMO* spacecraft early in 2013. In the following months, the *MMO* spacecraft had to pass a number of environmental tests like vibration and electro-magnetic compatibility under the supervision of Japanese space companies.

For *PICAM*, 2013 was mainly devoted to environmental, functional and performance test campaigns for the qualification model. Environmental testing started with the successful vibration and shock test in January, followed by the thermal vacuum (TV) test and the verification of the physical properties during summer. A non-conformance in the course of the TV test triggered an extensive review of the sensor design resulting in an improvement of various mechanical parts. The time in-between the environmental verification campaigns was used for intensive functional and performance test runs, which verified the sensor's behavior. The Qualification Model (Fig. 27) was finally delivered in October as a temporary FM replacement for system integration tests.

*Fig. 27: PICAM Qualification Model in its final configuration, mounted on the transport plate.*

In parallel, the FM campaign made good progress. Electronics including its box and the sensor mechanics became available by November. Exhaustive thermal balance tests in particular of the ion optics were carried out afterwards. The development of the detector electronics by the French partner LPP was again hampered by problems with the front-end ASIC. However, a final decision on the ASIC issue cleared the way for the detector assembly and testing as well as for the integration of the *PICAM* FM in 2014.

# Venus & Mars

Two terrestrial planets are located just inside, Venus at 0.7 AU (AU = Astronomical Unit, distance Earth-Sun), and just outside, Mars at 1.5 AU, of the Earth's orbit around the Sun. Venus has a radius only slightly smaller than Earth and is differentiated; it does, however, not exhibit an internal magnetic field. Mars has a radius about half as big as that of the Earth, is also differentiated, but only exhibits remnant surface magnetization of a now defunct internal dynamo. Venus is characterized by a very dense atmosphere, whereas Mars has a very tenuous one. Both planets generate a so-called induced magnetosphere by their interaction with the solar wind.

## Venus Express

ESA's first mission to Venus was launched in 2005. IWF takes the lead on one of the seven payload instruments, the magnetometer *VEX-MAG*, which measures the magnetic field vector with a cadence of 128 Hz. It maps the magnetic properties in the magnetosheath, the magnetic barrier, the ionosphere, and the magnetotail.

During 2013, the *Venus Express* spacecraft continued operating normally. The magnetometer remained ON during the whole year and collected magnetic field data both near Venus and in interplanetary space. Routine data processing and cleaning of the magnetic field measurements was undertaken for 1 Hz data. The software for data cleaning and process is robust and error-free. All data were cleaned and issued to the science community. Cleaning on 32 Hz data has been continued

for part of the data. Archiving of all available data has been carried out and all data have been delivered to ESA's Planetary Data System.

## InSight

NASA's *InSight* Mission to Mars (with an anticipated launch date 2016) is progressing according to plan. IWF is contributing to a self-penetrating probe, nicknamed "the mole", whose aim is to measure the planetary heat flux and the soil properties down to a depth of 5 m below the Martian surface. IWF is responsible for the investigation of the soil-mechanical aspects of the mole penetration.

## Physics

The solar wind interacts directly with the atmosphere of Venus in contrast to the situation at the Earth whose magnetic field protects the upper atmosphere. Still Venus' atmosphere is partially shielded by an induced magnetic field and it needs to be understood how effective that shield is. It is expected that the effectiveness varies with solar activity but current understanding of the solar wind interaction with Venus is derived from measurements at solar maximum only. *Venus Express*, with improved instrumentation, a different orbital trajectory, and observations at solar minimum, enables understanding the evolution of the Venus atmosphere caused by the solar wind interaction.

***Venusian flux ropes:*** Early *Pioneer* Venus observations during the solar maximum revealed that Venus' ionosphere exhibits two magnetic states depending on the solar wind dynamic pressure conditions: a magnetized ionosphere with a large-scale horizontal magnetic field; or an unmagnetized ionosphere with numerous small-scale thin structures, so-called flux ropes. Observations from *Venus Express* during solar minimum indicate yet another magnetic state of Venus' ionosphere, giant flux ropes in the magnetized ionosphere (Fig. 28).

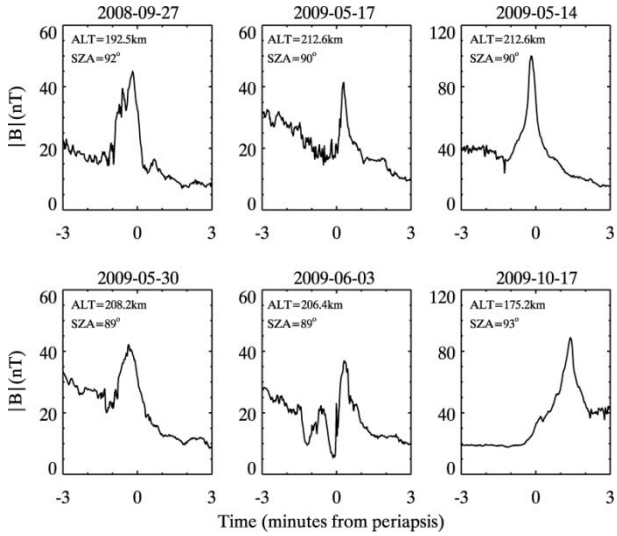


*Fig. 28: Examples of giant flux ropes observed in the magnetized ionosphere at Venus. The ALT and SZA are the altitude and solar zenith angle at periapsis.*

These giant flux ropes all have strong core fields and diameters of hundreds of kilometers, which is about the vertical dimension of the ionosphere. They are found to be quasi-stationary. The rope's axis is mainly quasi perpendicular to the solar wind flow direction and the core field orientation is highly correlated with the IMF BY direction. It is suggested that giant flux ropes are formed due to the solar wind interaction with Venus, most probably in the magnetotail, and later transported and deposited in the ionosphere at the terminator.

***Escape of the Martian protoatmosphere:*** Latest research in planet formation indicates that Mars formed within a few million years and remained a planetary embryo that never grew to a more massive planet. Using estimates for the initial water content of the planet's building blocks, the nebula-captured hydrogen envelope and catastrophically outgassed water dominated steam atmosphere during the solidification of Mars' magma ocean has been modeled. Then a hydrodynamic upper atmosphere model was applied to study the soft X-ray and extreme ultraviolet (XUV) driven thermal escape during the early active epoch of the young Sun. The solar XUV flux was 100 times higher than today. Combined with the low gravity of the planet, this results in Mars

having lost its nebular captured hydrogen envelope after the nebula gas evaporated, during a short 0.1–7.5 Myr period. After the solidification of early Mars' magma ocean, catastrophically outgassed volatiles in a range of 50–250 bar $H_2O$ and 10–55 bar $CO_2$ atmosphere could have been lost during 0.4–12 Myr (see Fig. 29) If the impact related energy flux of large planetesimals and small planetary embryos to the planet's surface lasted long enough the steam atmosphere could have been prevented from condensing. It can be expected that after the loss of the protoatmosphere during the most active XUV period of the young Sun, a secondary atmosphere may have evolved by a combination of volcanic outgassing and impacts 4:0±0:2 Gyr ago, when the solar XUV flux decreased to values less than 10 times of today's Sun.

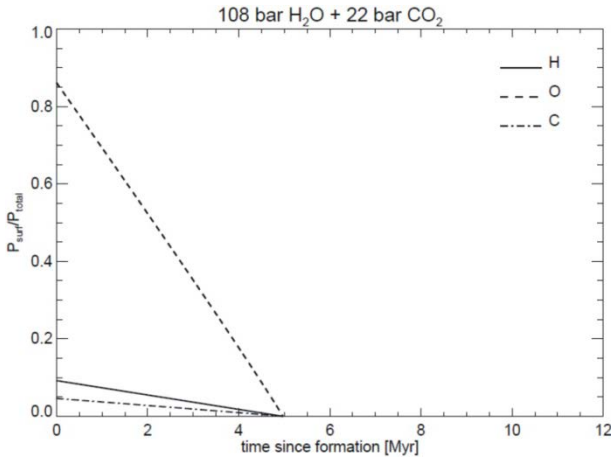


*Fig. 29: Example of the temporal evolution of the partial surface pressures normalized to the total initial surface pressure $P_{total}$ of an outgassed steam atmosphere with 108 bar $H_2O$ and 22 bar $CO_2$ surface pressure during about 5 Myr after its formation.*

# Jupiter & Saturn

Jupiter and Saturn are the two largest planets in the solar system. Because of their atmospheric composition they are called "gas giants". Both planets rotate rapidly (approximately 10 hours) and are strongly magnetized, with the Jovian field a multipole field tilted at 10° and the Kronian field almost dipolar and perfectly aligned with the rotational axis. The magnetospheres are dominated by internal plasma sources, generated by the large number of moons, particularly Io at Jupiter and Enceladus at Saturn. The gas giants are also strong sources of radio emissions.

## Cassini

The *Cassini* spacecraft is still orbiting Saturn, the second largest planet in our solar system. The 2013 spacecraft orbits were inclined by ~50°–60° with respect to Saturn's equatorial plane. In this year *Cassini* performed eight Titan flybys and its last close flyby of the Saturnian moon Rhea.

## JUICE

ESA's first Large-class mission *JUpiter ICy moons Explorer (JUICE)* is planned for launch in 2022 and arrival at Jupiter in 2030. It will spend at least three years making detailed observations of the giant gaseous planet Jupiter and three of its largest moons, Ganymede, Callisto and Europa. Its instruments were selected in February 2013. IWF was successful in obtaining CoI-ship for three different selected instrument packages. For the *Jupiter Magnetic Field Package (J-MAG)* IWF participates in the development of the baseline fluxgate magnetometers. The development of an additional scalar sensor, by IWF in collaboration with TU Graz, is defined as optional. A decision on the scalar sensor is expected for April 2014 as an outcome of the Instrument Preliminary Requirements Review of *J-MAG*. The *Particle Environment Package (PEP)* is a plasma package with sensors to characterize the plasma environment in the Jovian system and the composition of the exospheres of Callisto, Ganymede, and Europa. IWF participates in the *PEP* consortium on Co-I basis in the scientific studies related to the plasma interaction and exosphere formation of the Jovian satellites. Last but not least, IWF is responsible for the antenna calibration of the *Radio and Plasma Wave Investigation (RPWI)* instrument. Here, first numerical simulations of the antenna characteristics of the three *RPWI* monopoles

have been performed. The antenna triad was placed on the central spacecraft body and on the magnetometer boom to find the configuration with the best performance.

## Juno

*Juno* is a NASA mission to the gas giant Jupiter that was launched in 2011 and will enter into a Jovian orbit in 2016. On 9 October 2013 the spacecraft obtained a gravity-assist slingshot from an Earth flyby putting it on its way to Jupiter almost perfectly. *Juno* will be in a polar orbit, which is the first of its kind and is solely powered by solar panels, another first. Its scientific objectives are a.o. determining the water content in Jupiter's atmosphere, map the magnetic and gravity fields, and explore the magnetic pole regions, specifically the aurorae. IWF was involved in the antenna calibration of the *WAVES* instrument, which will investigate the auroral acceleration region and measure radio and plasma waves.

## Physics

***Periodic bursts of Jovian non-Io decametric radio emission (DAM):*** Three groups of periodic radio bursts in Jovian non-Io controlled DAM have been analyzed. The radio emission was recorded by *Cassini*, *Wind* and *STEREO* in the decametric frequency range. The main group is observed as a series of arc-like radio bursts with negative frequency drift (vertex-late bursts, Fig. 30 a) which reoccur with ~1.5% longer period than the Jovian magnetosphere rotation rate. The occurrence of these bursts is correlated with pulses of the solar wind ram pressure at Jupiter. In the second group the arc-like periodic radio bursts exhibit positive time-frequency drift (vertex-early bursts, Fig. 30 b). In contrast to the main group the vertex-early bursts reoccurred with the period close to the Jupiter rotation and were typically observed during 7-10 Jupiter rotations. The last observed group is of the rarely recorded non-arc periodic radio features in the form of a broad beamed radio emission, lacking clear discrete features (Fig. 30 c).

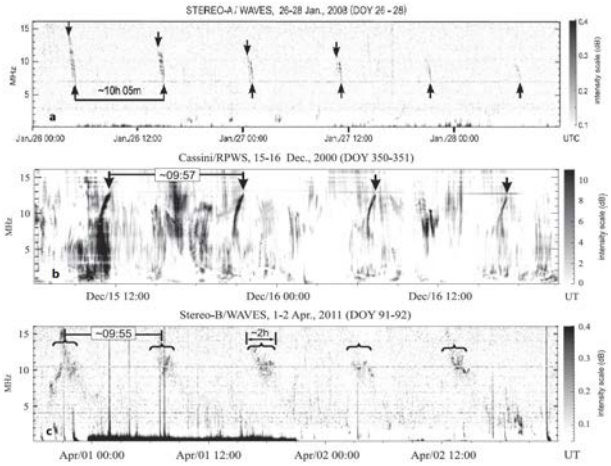


*Fig. 30: Examples of vertex-late (panel a), vertex-early (panel b) and non-arc (panel c) periodic radio bursts of Jovian non-Io DAM.*

***Comparative magnetotail flapping:*** Magnetotail flapping (the up-and-down wavy motion) is commonly observed in the Earth's magnetosphere. Now a comparison of flapping at the Earth and the two giant planets Jupiter and Saturn has been performed. Due to single spacecraft missions at the giant planets this can only be done through investigation of the current sheet normal of the magnetotail. A case can be made that magnetotail flapping also occurs at Jupiter and Saturn. Calculations of the wave period using generic magnetotail models show that the observed periods are much shorter than their theoretical estimates. However, this discrepancy can be caused by unknown input parameters for the tail models (e.g., current sheet thickness) and by possible Doppler shifting of the waves in the spacecraft frame through the fast rotation of the giant planets.

***Lightning in Saturn's atmosphere:*** Saturn's GWS (Great White Spot) of 2010/2011 was further investigated using data from the *Cassini* camera in combination with its *Radio and Plasma Wave Science (RPWS)* instrument. The GWS was a giant thunderstorm that raged in Saturn's northern hemisphere for about nine

months and emitted radio waves caused by lightning discharges. Fig. 31 displays *Cassini* images of the GWS which show the westernmost head region and the storm's long tail.

*RPWS* data indicated that the storm's head was the main center of lightning activity, but the region of active thunderstorm cells also extended eastward into the tail. This was confirmed by the first optical observation of flashes on Saturn's dayside located eastward of the head (see Fig. 31).

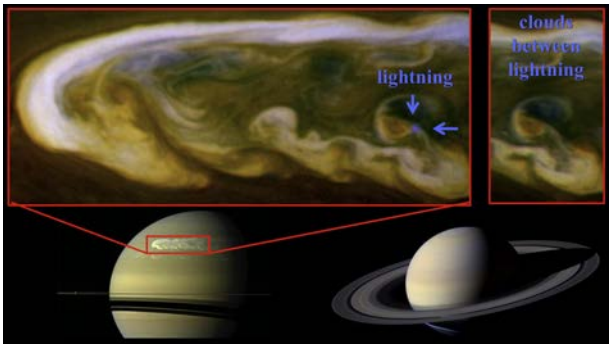


*Fig. 31: The upper part of this figure shows two Cassini images taken on 6 March 2011. The left panel shows a blue spot attributed to a lightning flash, which is absent in the right panel image taken half an hour later. The lower part of this figure displays two Saturn images to show the large extent of the Great White Spot (GWS).*

The head region periodically spawned anticyclonic vortices, and the optical flashes appeared in the cyclonic gaps between them where the atmosphere looked clear down to the level of deep clouds. The largest anticyclonic vortex in the tail drifted with a rate that was 2°/day slower than the head. Hence, after about half a year one caught up with the other, and it came to a head-vortex collision in mid-June 2011. This led to a significant decrease of lightning and convective activity, which became intermittent and finally ended in late August 2011.

# Comets

In recent years, successful space missions like *Giotto*, *VEGA*, *Stardust*, *Deep Impact*, and others have dramatically increased our knowledge on comets and their nuclei from flybys only. The next major milestone will be the arrival of *Rosetta* at comet 67P/Churyumov-Gerasimenko (short Chury) in 2014 and the landing of *Philae* on the comet's surface.

## Rosetta

ESA's *Rosetta* probe is continuing its already nine year long journey to comet Chury. Solar panels are the only energy source for the spacecraft, which do not supply enough energy around *Rosetta's* aphelion. Therefore, the craft has been placed into sleeping mode. After a successful wake-up call in January 2014, the commissioning phase for the instruments will start. *Rosetta* will arrive at the comet in summer 2014 and after an extensive surface mapping the *Philae* lander will be dropped onto the comet's nucleus. IWF participates in five instruments aboard both orbiter and lander and concentrates now on preparatory work for data evaluation and interpretation.

## Physics

*Cometary outgassing:* In view of the expected landing of *Philae* in November 2014 a theoretical model has been developed, describing the emission of gases from cometary crevasses. It includes both the possible transformation of amorphous ice into crystalline ice and the sublimation from the icy surface. Two qualitatively different cases have been studied: (i) free sublimation from the ice-filled crack and (ii) sublimation and diffusion through a thin dust mantle evolving over time.

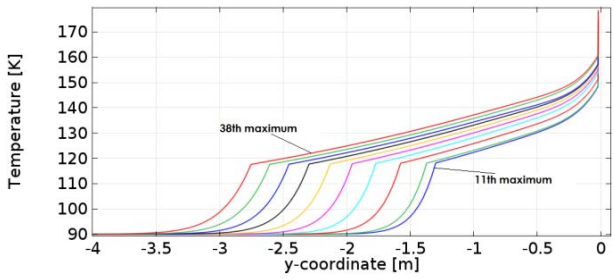


*Fig. 32: Temperature development at different depth levels in a cometary crevasse filled by water ice and covered by a thin dust mantle. The distance from the Sun is 2.7 AU, which corresponds to the solar distance of comet Chury at the expected landing time of Philae.*

Fig. 32 shows the evolution of the temperature over time for an ice-filled crack covered by a thin dust mantle. For the *MUPUS* experiment aboard *Philae* calibration measurements have been performed using an engineering model of the *MUPUS* penetrator in the cryo-vacuum chamber.

# Exoplanets

The field of exoplanet (i.e. planets around stars other than our Sun) research has developed strongly, in the past decade. Since the discovery of 51 Peg b, the first Jupiter-type gas giant outside our solar system, more than 1000 exoplanets, about 800 planetary systems with more than 170 multiple planet systems have been detected. Better observational methods have led to the finding of so-called super-Earths, some of them even inside the habitable zones of their host stars. However, the majority of super-Earths have low average densities, which indicate that they are surrounded by dense hydrogen envelopes or volatiles. By minimizing the uncertainties of the radii with the upcoming missions *CHEOPS* and *PLATO* densities and hence the structure of these planets will be better determined.

## CHEOPS

ESA's first Small-class mission *CHEOPS (CHaracterizing ExOPlanets Satellite)* will be the first space mission dedicated to characterize exoplanets in detail. It will focus on exoplanets with typical sizes ranging from Neptune down to Earth diameters orbiting bright stars, trying also to specify the components of their atmospheres. *CHEOPS* will be implemented under the leadership of the University of Bern, Switzerland, with Belgium, Italy, Sweden, UK, and Austria delivering substantial contributions. Austria will contribute the back-end-electronics, which contains the Digital Processing Unit (DPU) built by IWF Graz and the power supply for the entire electrical subsystem built by RUAG Space Austria in Vienna. The redundant DPU will handle the complete data traffic, control the camera and compress the data stream. In addition, it will conduct the thermal control for the optical elements except the image sensor itself. It has a planned mission lifetime of 3.5 years, during which it will observe approx. 500 bright stars and characterize their planets.

## Physics

***Exoplanet atmosphere-magnetosphere studies:*** The discovery of transiting super-Earths with inflated radii and known masses, such as Kepler-11b-f, GJ 1214b and 55 Cnc e, indicates that these exoplanets did not lose their nebula-captured hydrogen-rich, degassed or impact-delivered protoatmospheres by atmospheric escape processes. The hydrodynamic blow-off escape criteria of seven hydrogen-dominated super-Earths were studied by applying a time-dependent numerical algorithm which solves the 1D fluid equations for mass, momentum and energy conservation. Results as those shown in Fig. 33 indicate that the upper atmospheres of super-Earths can expand to large distances, so that, except for Kepler-11c, all of them experience atmospheric mass-loss due to Roche lobe overflow.

The atmospheric mass loss of the studied super-Earths is one to two orders of magnitude lower compared to that of "hot Jupiters" such as HD 209458b, which are exposed to higher XUV fluxes at closer orbital distances. The loss rates of these exoplanets are too weak so they cannot lose their hydrogen envelopes during their remaining lifetimes. These results are also supported by stellar wind induced ion pick-up studies of hydrogen envelopes of super-Earths. Using a Monte Carlo simulation of stellar wind-plasma interaction, it is found that thermal escape rates of hydrodynamically outward flowing neutral atoms exceed the non-thermal $H^+$ loss rates up to an order of magnitude. Therefore, it is

possible that super-Earths at orbital distances greater than 0.1 AU may not lose their primordial atmosphere.

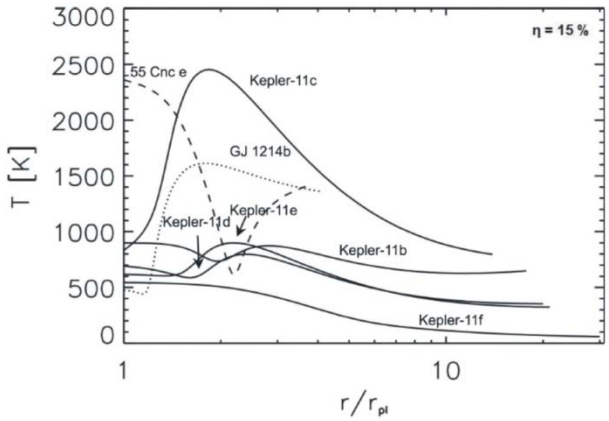


*Fig. 33: Modeled temperature profiles of the super-Earths 55 Cnc e, GJ 1214b, Kepler-11b-f from the lower thermosphere up to the Roche lobe distance $r_{L1}$ for a heating efficiency with $\eta$=15%.*

Furthermore, the XUV-heated outward expanding upper atmospheres may also be influenced by the presence of a magnetic field. The exoplanet host star's high radiation field will ionize a part of the upper atmosphere. The interaction between the nonhydrostatically outflowing atmospheric plasma and an intrinsic planetary magnetic dipole field leads to the formation of an equatorial current-carrying magnetodisk. The presence of a magnetodisk influences the topology of the exoplanet's magnetosphere and changes the standoff distance of the magnetopause. The basic features of the formation of an exoplanet's magnetodisk have been studied in the laboratory (Fig. 34). A localized central source produces plasma that expands outward from the surface of the dipole and inflates the magnetic field. The observed structure of magnetic fields, electric currents, and plasma density indicates the formation of a relatively thin current disk extending beyond the Alfvénic point. At the edge of the current disk, the induced magnetic field is several times larger than the field of the initial dipole.

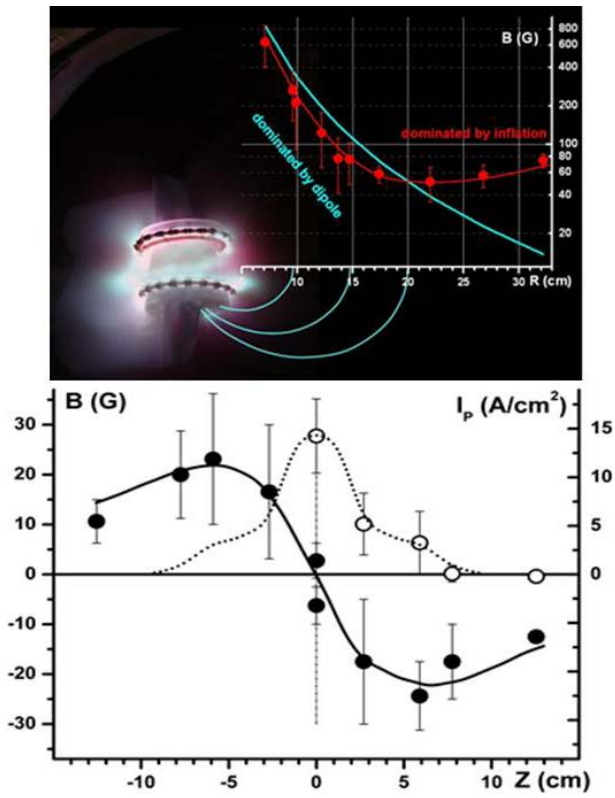


*Fig. 34: Experimental setup (upper panel) and profiles of the radial component $\delta B_R$ (full circles, left axis) and current in plasma (open circles, right axis) across the equatorial plane at a distance of R≈20 cm (lower panel).*

# Testing & Manufacturing

Instruments onboard spacecraft are exposed to harsh environments, e.g., vacuum, large temperature ranges, radiation and high mechanical loads during launch. Furthermore, these instruments are expected to be highly reliable, providing full functionality over the entire mission time, which could last for even more than ten years.

## Vacuum Chambers

The *Small Vacuum Chamber* is a manually controlled, cylindrical vacuum chamber (160 mm diameter, 300 mm length) for small electronic components or printed circuit boards. It features a turbo molecular pump and a rotary dry scroll forepump. A pressure level of $10^{-10}$ mbar can be achieved.

The *Medium Vacuum Chamber* has a cylindrical stainless steel body with the overall length of 850 mm and a diameter of 700 mm. A dry scroll forepump and a turbo molecular pump provide a pressure level of about $10^{-7}$ mbar. A target manipulator with two axes and an ion beam source are installed. This chamber mainly serves for functional tests of the ion mass spectrometer for *BepiColombo*.

The *Large Vacuum Chamber* (Fig. 35) has a horizontal cylindrical stainless steel body and door, a vision panel, two turbo molecular pumps and a dry scroll forepump. A pressure of $10^{-7}$ mbar can be achieved. The cylinder has a diameter of 650 mm and a length of 1650 mm. During shutdown the chamber is vented with nitrogen. A target manipulator inside the chamber allows for computer-controlled rotation of the target around three mutually independent perpendicular axes. The vacuum chamber is enclosed by a permalloy layer for magnetic shielding. To enable the baking of structures and components (to outgas volatile products and unwanted contaminations), the chamber is equipped with a heater around the circumference.

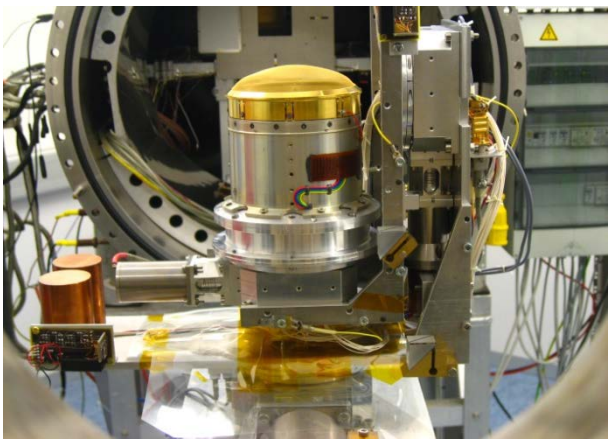

*Fig. 35: The electron gun of the MMS Electron Drift Instrument (mounted onto the three axes movable platform inside the vacuum chamber to perform the calibration.*

The *Thermal Vacuum Chamber* is fitted with a turbo molecular pump, a dry scroll forepump, and an ion getter pump, which together achieve a pressure level of $10^{-6}$ mbar and allow quick change of components or devices to be tested. A thermal plate installed in the chamber and liquid nitrogen are used for thermal cycling in a temperature range between −90 °C and +140 °C. The vertically oriented cylindrical chamber allows a maximum experiment diameter of 410 mm and a maximum height of 320 mm.

The *Surface Laboratory Chamber* is dedicated to surface science research. It has a diameter of 400 mm and a height of 400 mm, extendable up to 1200 mm. One rotary vane pump and one turbo-molecular pump achieve a minimum pressure of $10^{-5}$ mbar. With an ex-

ternal thermostat the chamber temperature can be optionally controlled between -90°C and +50°C.

The *Sample Chamber* contains an 8µ particle filter and allows measurements of grain sample electrical permittivity. One rotary vane pump achieves a minimum pressure of $10^{-3}$ mbar.

## Other Test Facilities

The *Temperature Test Chamber* allows verifying the resistance of electronic components and circuits to most temperature conditions that occur under natural conditions, i.e., -40 °C to +180 °C. The chamber has a test space of 190 liters and is equipped with a 32-bit control and communication system.

The *Penetrometry Test Stand* is designed to measure mechanical soil properties, like bearing strength.

The *UV Exposure Facility* is capable to produce radiation between 200-400 nm (UV-A, UV-B, UV-C).

*Magnetometer calibration:* A three-layer magnetic shielding made from mu-metal is used for all basic magnetometer performance and calibration tests. The remaining DC field in the shielded volume is <10 nT and the remaining field noise is <2 pT/√Hz at 1 Hz. A special Helmholtz coil system allows generating field vectors of up to +/-30000 nT around the sensor under test.

The *Magnetometer Temperature Test Facility* is used to test magnetic field sensors between -170 °C and +220 °C in a low field and low noise environment. Liquid nitrogen is the base substance for the regulation which is accurate to +/-0.1 °C. A magnetic field of up to +/-100000 nT can be applied to the sensor during the test cycles.

## Flight Hardware Production

*Clean room:* Class 10000 (according to U.S. Federal Standard 209e) certified laboratory with a total area of 30 $m^2$. The laboratory is used for flight hardware assembling and testing and accommodates up to six engineers.

*Clean bench:* The laminar flow clean bench has its own filtered air supply. It provides product protection by ensuring that the work piece in the bench is exposed only to HEPA-filtered air (HEPA = High Efficiency Particulate Air). The internal dimensions are 118 x 60 x 56 $cm^3$.

*Vapor phase and IR soldering machine:* The vapor phase soldering machine is suitable for mid size volume production. The maximum board size is 340x300x80 $mm^3$. Vapor phase soldering is currently the most flexible, simplest and most reliable method of soldering. It is ideally suited for all types of surface mounted device (SMD) components and base materials. It allows processing of all components without the need of any complicated calculations or having to maintain temperature profiles. For placing of fine pitch parts and rework of electronic boards an infrared soldering and precision placing system is used.

# Outreach

## Public Outreach

IWF is actively engaged in science education and public outreach. Throughout the year, many different groups and school classes (from WIKU Graz, VS BIPS Krones, NMS 1 Deutschlandsberg, Akademisches Gymnasium, NMS Krottendorf) visited the institute.

In January, ARGE KIWI (working group "Children and Science") invited more than 100 children from VS Berlinerring, VS Gösting, VS Viktor Kaplan, NMS Andritz, and NMS St. Johann to visit both IWF and the laser station at Lustbühel Observatory in the frame of the project "Wissen schaf[f]t Durchblick".

*Fig. 36: LR Kristina Edlinger-Ploder, initiator Christoph Kürbisch, and IWF Director Wolfgang Baumjohann (from right to left) had the honorable task to cut the ribbon between Mercury, Venus, Earth, and Mars.*

On 24 May, an "Einstein-Junior" families' day was organized at IWF. About 100 people, among them 30 children, learned about our solar system in different talks, guided tours through the labs, and an extraordinary rap performed by Petra Huber from the Kinderbüro of the City of Graz and her team of five very enthusiastic young ladies and gentlemen. As celebratory end of this day, the Planetary Garden, initiated by IWF employee Christoph Kürbisch, was opened (Fig. 36).

In June, the ÖAW Work Council organized an excursion for all employees to Graz, which included a visit to IWF.

In September IWF hosted the UN/Austria Symposium on "Space Weather Data, Instruments and Models: Looking Beyond the International Space Weather Initiative (ISWI)".

From 15-24 November the ScienceCenter Netzwerk organized the Austrian "Themenwoche Weltraum", in which IWF also participated. Again approximately 100 space enthusiasts were guided through the institute and the SLR station.

From 9-13 December, "Post Alpach" was held at Schloss St. Martin. Günter Kargl and Martin Volwerk served as tutors and organized a visit to the institute for the 16 students.

*Fig. 37: Wolfgang Baumjohann surrounded by students from HLFS Urspung (Photo: HLFS Ursprung).*

On 16 December, Bernhard Stehrer from HLFS Urspung, Salzburg, travelled to Graz together with a small group of committed young people who wanted to learn more about the institute and space research in general. They were guided through the labs and interviewed the

IWF Director about intelligent life in the universe (Fig. 37).

In the framework of the "FEMtech" program of FFG, four young ladies from KFU and TU Graz worked at IWF for two and four months, respectively. During summer time, five high-school students from BG/BRG Weiz (verification and evaluation of the accuracy and functionality of miniaturized magnetic field and acceleration sensors), HTL Weiz (data analysis of the El Niño phenomenon in the 19th century), HTL-BULME Graz-Gösting (reference box for personnel ground tester and break-out box for a dedicated interface standard), Akademisches Gymnasium (low frequency wave propagation problems), and BORG Deutschlandsberg (simulation of the influence of sensor materials on the magnetic field measurements of *CDSM)* performed an internship at IWF under the "Talente-Praktika" program of FFG. Additionally, a 16 year old girl from the European School of Brussels spent two weeks at IWF to get some work experience.

Throughout the year, several URANIA series of lectures on the topics "From the outer solar system to exoplanets" and "The world of astronomy - The history of matter" were held by members of the institute.

Last but not least, in June the "Topic of the Month" of the Austrian Academy of Sciences was "Aurora, Solar Wind, and Magnetic Field Turbulences", with contributions by Bruno Besser, Rumi Nakamura, and Evgeny Panov.

# Awards and Recognition

On 13 November, the Institute of Radio Astronomy of the National Academy of Sciences of Ukraine awarded an Honorary Doctorate to Helmut O. Rucker for his "outstanding scientific merits and long-term fruitful collaboration with Ukrainian radio astronomers".

On 18 November, Mayor Siegfried Nagl awarded the F. Schmiedl Forschungspreis to Andreas Pollinger for his TU Graz doctoral thesis "Development and Evaluation of a Control Unit for the Coupled Dark State-Magnetometer" (Fig. 38).

*Fig. 38: On 18 November Andreas Pollinger was awarded the F. Schmiedl Forschungspreis by Mayor Siegfried Nagl (Photo: Stadt Graz / Thomas Fischer).*

# Meetings

Wolfgang Baumjohann served as Vice Director and Rumi Nakamura on the Program Committee of the Summer School Alpbach, which took place from 16 to 25 July and was dedicated to „Space Weather: Science, Missions and Systems". Every year, 60 students and about 25 lecturers and tutors from among ESA's member states are invited to this meeting.

Additionally, W. Baumjohann, M.L. Khodachenko, G. Kirchner, H. Lammer, R. Nakamura, Y. Narita, and H.O. Rucker were members of program and/or scientific organizing committees for 11 international conferences/workshops. O. Baur, M.Y. Boudjada, G. Fischer, G. Kargl, G. Kirchner, H. Lammer, R. Nakamura, Y. Narita, M. Scherf, G. Stangl, and Z. Vörös organized 20 sessions at international meetings.

# Lecturing

IWF members are actively engaged in teaching at three universities and two universities of applied sciences. In summer 2013 and in the current winter term 2013/2014 the following lectures are given:

## KFU Graz

AK Weltraumphysik und Aeronomie (Kömle)

Data processing in solar and space physics (Nakamura et al.)

Introduction to Geophysics and Planetary Physics (Kargl et al.)

Introduction to Plasma Physics (Rucker)

Messmethoden der Weltraumphysik und Aeronomie (Kargl, Rucker)

Planetenmagnetosphären (Rucker)

Schwerkraft, Figur, Seismik und Aufbau der Erde (Kömle)

Spezialvorlesung zur Theoretischen Physik: Plasmatheorie (Wellen) (Biernat)

## TU Graz

Advanced Satellite Geodesy (Baur et al.)

Antennen und Wellenausbreitung (Riedler et al.)

Design and Development of Space Qualified Hardware (Magnes)

Digitale Audiotechnik, Labor (D. Fischer, Magnes)

Fortgeschrittene Weltraumplasmaphysik (Baumjohann)

GGOS and Reference Systems (Baur et al.)

Hochfrequenztechnik (Riedler et al.)

Introduction to Satellite Geodesy (Sünkel)

Measurement of Planetary and Interplanetary Magnetic Fields (Schwingenschuh)

Signalprozessortechnik (Magnes)

## TU Braunschweig

Einführung in die Astroteilchenphysik (Narita)

Teilchenphysikalische Kosmologie (Narita)

## FH Joanneum

Mathematik 1 für Informatik (Lichtenegger)

## FH Wiener Neustadt

Space Environment and Interactions (D. Fischer, Plaschke)

## Advanced Course

The four semesters Master Studies curriculum „Space Sciences and Earth from Space“ as a cooperative curriculum within the frame of NAWI (KFU and TU) Graz was established in 2011 and continues with starts each winter term. At present 24 students have enrolled.

# Theses

Besides lecturing, members of the institute are supervising Bachelor, Diploma, Master and Doctoral Theses. In 2013, the following supervised theses have been completed:

Chaghiashvili, T.: Flare-Related Dynamics of Active Regions, Diploma Thesis, Ilia State University, Georgia, 29 pages (2013).

Edl, M.: Magnetotail Current Sheet Crossings Observed by Cluster Four-Spacecraft Measurements, Bachelor Thesis, Universität Graz, 33 pages (2013)

Klinger, B.: Lunar Gravity Field Recovery: GRAIL Simulations and Real Data Analysis, Diploma Thesis, TU Graz, 102 pages (2013).

Krauss, S.: Response of the Earth's thermosphere during extreme solar events. A contribution of satellite observations to atmospheric evolution studies, Doctoral Thesis, TU Graz, 119 pages (2013).

Krebl, B.L.: Numerical model of the gas flow and temperature development in an ice filled crevasse on the surface of a comet's nucleus, Diploma Thesis, Universität Graz, 101 pages (2013).

Philishvili, E.: Active Region Dynamics During Solar Flare, Diploma Thesis, Ilia State University, Georgia, 50 pages (2013).

Pollinger, A.: Development and Evaluation of a Control Unit for the Coupled Dark State Magnetometer, Doctoral Thesis, TU Graz, 98 pages (2013).

Rief, G.: Numerical Calibration of the Cassini RPWS Antenna System, Diploma Thesis, Universität Graz, 80 pages (2013).

Teubenbacher, R.: Determination of Spin-Axis Offset of a Fluxgate Magnetometer Using Data from the Electron Drift Instrument Onboard the Cluster Satellite, Diploma Thesis, TU Graz, 78 pages (2013).

Topf, F.: Prototype of a Portal for Scientific Data Access Based on Scala, Master Thesis, FH Campus 02 Graz, 133 pages (2013)

Wu, M.Y.: Study of Earth Magnetospheric Plasma Waves, Doctoral Thesis, University of Science and Technology of China, Hefei, 106 pages (2013).

# Publications

## Refereed Articles


Al-Haddad, N., T. Nieves-Chinchilla, N.P. Savani, C. Möstl, K. Marubashi, M.A. Hidalgo, I.I. Roussev, S. Poedts, C.J. Farrugia: Magnetic field configuration models and reconstruction methods for interplanetary Coronal Mass Ejections, *Solar Phys.*, **284**, 129-149 (2013)

Almenara, J.M., F. Bouchy, P. Gaulme, M. Deleuil, M. Havel, D. Gandolfi, H.J. Deeg, G. Wuchterl, T. Guillot, B. Gardes, T. Pasternacki, S. Aigrain, R. Alonso, M. Auvergne, A. Baglin, A.S. Bonomo, P. Bordé, J. Cabrera, S. Carpano, W.D. Cochran, Sz. Csizmadia, C. Damiani, R.F. Diaz, R. Dvorak, M. Endl, A. Erikson, S. Ferraz-Mello, M. Fridlund, G. Hébrard, M. Gillon, E. Guenther, A. Hatzes, A. Léger, H. Lammer, P.J. MacQueen, T. Mazeh, C. Moutou, M. Ollivier, A. Ofir, M. Pätzold, H. Parviainen, D. Queloz, H. Rauer, D. Rouan, A. Santerne, B. Samuel, J. Schneider, L. Tal-Or, B. Tingley, J. Weingrill: Transiting exoplanets from the CoRoT space mission XXIV. CoRoT-25b and CoRoT-26b: Two low-density giant planets, *Astron. Astrophys.*, **555**, A118 (2013)

Angelopoulos, V., A. Runov, X.-Z. Zhou, D.L. Turner, S.A. Kiehas, S.-S. Li, I. Shinohara: Electromagnetic energy conversion at reconnection fronts, *Science*, **341**, 1478-1482 (2013)

Antonov, V.M., E.L. Boyarinsev, A.A. Boyko, Yu.P. Zakharov, A.V. Melekhov, A.G. Ponomarenko, V.G. Posukh, I.F. Shaikhislamov, M.L. Khodachenko, H. Lammer: Inflation of a dipole field in laboratory experiments: Toward an understanding of magnetodisk formation in the magnetosphere of a Hot Jupiter, *Astrophys. J.*, **769**, 28 (2013)

Arkhypov, O.V., H.O. Rucker: Decametric modulation lanes as a probe for inner Jovian magnetosphere, *Icarus*, **226**, 1214-1224 (2013)

Arkhypov, O.V., O.V. Antonov, M.L. Khodachenko: Solar activity and deep convection modeling, *Solar Phys.*, **282**, 39-50 (2013)

Artemyev, A.V., A.A. Petrukovich, A.G. Frank, R. Nakamura, L.M. Zelenyi: Intense current sheets in the magnetotail: Peculiarities of electron physics, *J. Geophys. Res.*, **118**, 2789-2799 (2013)

Artemyev, A.V., A.A. Petrukovich, R. Nakamura, L.M. Zelenyi: Profiles of electron temperature and Bz along Earth's magnetotail, *Ann. Geophys.*, **31**, 1109-1114 (2013)

Baur, O.: Greenland mass variation from time-variable gravity in the absence of GRACE, *Geophys. Res. Lett.*, **40**, 4289-4293 (2013)

Baur, O.: Parameter estimation by means of genetic algorithms: Potential and limitations from a geodetic perspective, *Allgemeine Vermessungsnachrichten*, **120**, 203-209 (2013)

Baur, O., M. Kuhn, W.E. Featherstone: Continental mass change from GRACE over 2002-2011 and its impact on sea level, *J. Geodesy*, **87**, 117-125 (2013)

Bertucci, C., N. Romanelli, J.Y. Chaufray, D. Gomez, C. Mazelle, M. Delva, R. Modolo, F. González-Galindo, D.A. Brain: Temporal variability of waves at the proton cyclotron frequency upstream from Mars: Implications for Mars distant hydrogen exosphere, *Geophys. Res. Lett.*, **40**, 3809-3813 (2013)

Birn, J., M. Hesse, R. Nakamura, S. Zaharia: Particle acceleration in dipolarization events, *J. Geophys. Res.*, **118**, 1960-1971 (2013)

Birn, J., R. Nakamura, M. Hesse: On the propagation of blobs in the magnetotail: MHD simulations, *J. Geophys. Res.*, **118**, 5497-5505 (2013)

Bisikalo, D., P. Kaygorodov, D. Ionov, V. Shematovich, H. Lammer, L. Fossati: Three-dimensional gas dynamic simulation of the interaction between the exoplanet WASP-12b and its host star, *Astrophys. J.*, **764**, 19 (2013)

Bonnet, J.-Y., R. Thissen, M. Frisari, V. Vuitton, E. Quirico, F.-R. Orthous-Daunay, O. Dutuit, L.

LeRoy, N. Fray, H. Cottin, S.M. Hörst, R.V. Yelle: Compositional and structural investigation of HCN polymer through high resolution mass spectrometry, *Int. J. Mass Spectrom.*, **354–355**, 193–203 (2013)

Cao, J.B., X.H. Wei, A.Y. Duan, H.S. Fu, T.L. Zhang, H. Reme, I. Dandouras: Slow magnetosonic waves detected in reconnection diffusion region in the Earth's magnetotail, *J. Geophys. Res.*, **118**, 1659–1666 (2013)

Cao, J.B., Y. Ma, G. Parks, H. Reme, I. Dandouras, T.L. Zhang: Kinetic analysis of the energy transport of bursty bulk flows in the plasma sheet, *J. Geophys. Res.*, **118**, 313–320 (2013)

Comisel, H., D. Verscharen, Y. Narita, U. Motschmann: Spectral evolution of two-dimensional kinetic plasma turbulence in the wavenumber-frequency domain, *Phys. Plasmas*, **20**, 090701 (2013)

Davies, J.A., C.H. Perry, R.M.G.M. Trines, R.A. Harrison, N. Lugaz, C. Möstl, Y.D. Liu, K. Steed: Establishing a stereoscopic technique for determining the kinematic properties of solar wind transients based on a generalized self-similarly expanding circular geometry, *Astrophys. J.*, **777**, 167 (2013)

Denisenko, V.V., M. Ampferer, E.V. Pomozov, A.V. Kitaev, W. Hausleitner, G. Stangl, H.K. Biernat: On electric field penetration from ground into the ionosphere, *J. Atmos. Sol.-Terr. Phys.*, **102**, 341–353 (2013)

Du, J., C. Wang, T.L. Zhang, E. Kallio: Asymmetries of the magnetic field line draping shape around Venus, *J. Geophys. Res.*, **118**, 6915–6920 (2013)

Dubinin, E., M. Fraenz, J. Woch, T.L. Zhang, Y. Wei, A. Fedorov, S. Barabash, R. Lundin: Toroidal and poloidal magnetic fields at Venus. Venus Express observations, *Planet. Space Sci.*, **87**, 19–29 (2013)

Dubinin, E., M. Fraenz, T.L. Zhang, J. Woch, Y. Wei, A. Fedorov, S. Barabash, R. Lundin: Plasma in the near Venus tail: Venus Express observations, *J. Geophys. Res.*, **118**, 7624–7634 (2013)

Dutuit, O., N. Carrasco, R. Thissen, V. Vuitton, C. Alcaraz, P. Pernot, N. Balucani, P. Casavecchia, A. Canosa, S. Le Picard, J.-C. Loison, Z. Herman, J. Zabka, D. Ascenzi, P. Tosi, P. Franceschi, S.D. Price, P. Lavvas: Critical review of N, N+, N2+, N++ and N2++ main production processes and reactions of relevance to Titan's atmosphere, *Astrophys. J. Suppl. Ser.*, **204**, 20 (2013)

Dyudina, U.A., A.P. Ingersoll, S.P. Ewald, C.C. Porco, G. Fischer, Y. Yair: Saturn's visible lightning, its radio emissions, and the structure of the 2009–2011 lightning storms, *Icarus*, **226**, 1020–1037 (2013)

Erkaev, N.V., H. Lammer, P. Odert, Y.N. Kulikov, K.G. Kislyakova, M.L. Khodachenko, M. Güdel, A. Hanslmeier, H. Biernat: XUV-exposed, non-hydrostatic hydrogen-rich upper atmospheres of terrestrial planets. Part I: Atmospheric expansion and thermal escape, *Astrobiol.*, **13**, 1011–1029 (2013)

Friedrich, M., K.M. Torkar, U.-P. Hoppe, T.-A. Bekkeng, A. Barjatya, M. Rapp: Multi-instrument comparisons of D-region plasma measurements, *Ann. Geophys.*, **31**, 135–144 (2013)

Golbraikh, E., M. Gedalin, M. Balikhin, T.L. Zhang: Large amplitude nonlinear waves in Venus magnetosheath, *J. Geophys. Res.*, **118**, 1706–1710 (2013)

Goyal, R., R.P. Sharma, M.L. Goldstein, N.K. Dwivedi: Nonlinear interaction of proton whistler with kinetic Alfven wave to study solar wind turbulence, *Phys. Plasmas*, **20**, 122308 (2013)

Guo, J.G., J.K. Shi, Z.W. Cheng, Z.Y. Zhang, Z. Wang, T.L. Zhang, Z.X. Liu, M. Dunlop: Variation of dependence of the cusp location at different altitude on the dipole tilt, *Chin. Sci. Bull.*, **58**, 3541–3545 (2013)

Hartinger, M.D., D.L. Turner, F. Plaschke, V. Angelopoulos, H. Singer: The role of transient ion foreshock phenomena in driving Pc5 ULF wave activity, *J. Geophys. Res.*, **118**, 299–312 (2013)

Hietala, H., F. Plaschke: On the generation of magnetosheath high-speed jets by bow shock ripples, *J. Geophys. Res.*, **118**, 7237–7245 (2013)

Juusola, L., M. Kubyshkina, R. Nakamura, T. Pitkänen, O. Amm, K. Kauristie, N. Partamies, H. Rème, K. Snekvik, D. Whiter: Ionospheric signatures of a plasma sheet rebound flow during a substorm onset, *J. Geophys. Res.*, **118**, 350–363 (2013)

Kiehas, S.A., V. Angelopoulos, A. Runov, S.-S. Li: On the azimuthal size of flux ropes near lunar orbit, *J. Geophys. Res.*, **118**, 4415–4424 (2013)

Kirchner, G., F. Koidl, F. Friederich, I. Buske, U. Völker, W. Riede: Laser measurements to space debris from Graz SLR station, *Adv. Space Res.*, **51**, 21–24 (2013)

Kislyakova, K.G., H. Lammer, M. Holmstrom, M. Panchenko, P. Odert, N.V. Erkaev, M. Leitzinger, M.L. Khodachenko, Y.N. Kulikov, M. Güdel, A. Hanslmeier: XUV-exposed, non-hydrostatic hydrogen-rich upper atmospheres of terrestrial planets. Part II: Hydrogen coronae and ion escape, *Astrobiol.*, **13**, 1030–1048 (2013)

Kömle, N.I., W. Macher, G. Kargl, M.S. Bentley: Calibration of non-ideal thermal conductivity sensors, *Geosci. Instrum. Method. Data Syst.*, **2**, 151–156 (2013)

Konovalenko, A.A., A.A. Stanislavsky, H.O. Rucker, A. Lecacheux, G. Mann, J.-L. Bougeret, M.L. Kaiser, C. Briand, P. Zarka, E.P. Abranin, V.V. Dorovsky, A.A. Koval, V.N. Melnik, D.V. Mukha, M. Panchenko: Synchronized observations by using the STEREO and the largest ground-based decametre radio telescope, *Exp. Astron.*, **36**, 137–154 (2013)

Konovalenko, A.A., N.N. Kalinichenko, H.O. Rucker, A. Lecacheux, G. Fischer, P. Zarka, V.V. Zakharenko, K.Y. Mylostna, J.-M. Grießmeier, E.P. Abranin, I.S. Falkovich, K.M. Sidorchuk, W.S. Kurth, M.L. Kaiser, D.A. Gurnett: Earliest recorded ground-based decameter wavelength observations of Saturn's lightning during the giant E-storm detected by Cassini spacecraft in early 2006, *Icarus*, **224**, 14–23 (2013)

Korovinskiy, D.B., A. Divin, N.V. Erkaev, V.V. Ivanova, I.B. Ivanov, V.S. Semenov, G. Lapenta, S. Markidis, H.K. Biernat, M. Zellinger: MHD modeling of the double-gradient (kink) magnetic instability, *J. Geophys. Res.*, **118**, 1146–1158 (2013)

Krebl, B.L., N.I. Kömle: A two-dimensional model of crevasses formed by cometary activity, *Planet. Space Sci.*, **87**, 46–65 (2013)

Kucharski, D., G. Kirchner, H.-C. Lim, F. Koidl: New results on spin determination of nanosatellite BLITS from High Repetition Rate SLR data, *Adv. Space Res.*, **51**, 912–916 (2013)

Kucharski, D., H.-C. Lim, G. Kirchner, J.-Y. Hwang: Spin parameters of LAGEOS-1 and LAGEOS-2 spectrally determined from Satellite Laser Ranging data, *Adv. Space Res.*, **52**, 1332–1338 (2013)

Kucharski, D., T. Otsubo, G. Kirchner, H.-C. Lim: Spectral filter for signal identification in the kHz SLR measurements of the fast spinning satellite Ajisai, *Adv. Space Res.*, **52**, 930–935 (2013)

Kucharski, D., T. Otsubo, G. Kirchner, H.-C. Lim: Spectral response of Experimental Geodetic Satellite determined from high repetition rate SLR data, *Adv. Space Res.*, **51**, 162–167 (2013)

Lammer, H., E. Chassefiere, O. Karatekin, A. Morschhauser, P.B. Niles, O. Mousis, P. Odert, U.V. Möstl, D. Breuer, V. Dehant, M. Grott, H. Gröller, E. Hauber, L.B.S. Pham: Outgassing history and escape of the Martian atmosphere and water inventory, *Space Sci. Rev.*, **174**, 113–154 (2013)

Lammer, H., M. Blanc, W. Benz, M. Fridlund, V. Coudé. du Foresto, M. Güdel, H. Rauer, S. Udry, R.-M. Bonnet, M. Falanga, D. Charbonneau, R. Helled, W. Kley, J. Linsky, L.T. Elkins-Tanton, Y. Alibert, E. Chassefière, T. Encrenaz, A.P. Hatzes, D. Lin, R. Liseau, W. Lorenzen, S.N. Raymond: The science of exoplanets and their systems, *Astrobiol.*, **13**, 793–813 (2013)

Lammer, H., N.V. Erkaev, P. Odert, K.G. Kislyakova1, M. Leitzinger, M.L. Khodachenko: Probing the blow-off criteria of hydrogen-rich 'super-Earths', *MNRAS*, **430**, 1247–1256 (2013)

Leinweber, H.K., C.T. Russell, K. Torkar: Precise calculation of current densities via four spinning spacecraft in a tetrahedron configuration, *IEEE Trans. Magnetics*, **49**, 5264–5269 (2013)

Li, S.-S., V. Angelopoulos, A. Runov, S.A. Kiehas, X.-Z. Zhou: Plasmoid growth and expulsion revealed by two-point ARTEMIS observations, *J. Geophys. Res.*, **118**, 2133–2144 (2013)

Lu, H.Y., J.B. Cao, M. Zhou, H.S. Fu, R. Nakamura, T.L. Zhang, Y.V. Khotyaintsev, Y.D. Ma, D. Tao: Electric structure of dipolarization fronts associated with interchange instability in the magnetotail, *J. Geophys. Res.*, **118**, 6019–6025 (2013)

Lu, Q., L. Shan, T.L. Zhang, G.P. Zank, Z. Yang, M. Wu, A. Du, S. Wang: The role of pickup ions on the structure of the Venusian bow shock and its implications for the termination shock, *Astrophys. J.*, **773**, L24 (2013)

Macher, W., N.I. Kömle, M.S. Bentley, G. Kargl: The heated infinite cylinder with sheath and two

thermal surface resistance layers, *Int. J. Heat Mass Transfer.*, **57**, 528–534 (2013)

Masunaga, K., Y. Futaana, G. Stenberg, S. Barabash, T.L. Zhang, A. Fedorov, S. Okano, N. Terada: Dependence of O+ escape rate from the Venusian upper atmosphere on IMF directions, *Geophys. Res. Lett.*, **40**, 1682–1685 (2013)

Moutou, C., M. Deleuil, T. Guillot, A. Baglin, P. Bordé, F. Bouchy, J. Cabrera, S. Csizmadia, H.J. Deeg, J.M. Almenara, M. Auvergne, S. Barros, A. Bonomo, C. Damiani, R. Díaz, G. Hébrard, A. Léger, G. Montagnier, M. Ollivier, D. Rouan, A. Santerne, J. Schneider, A. Erikson, E. Guenther, A. Hatzes, M. Pätzold, A. Ofir, H. Rauer, G. Wüchterl, R. Alonso, H. Parviainen, B. Tingley, S. Carpano, D. Gandolfi, M. Fridlund, R. Dvorak, H. Lammer, J. Weingrill, T. Mazeh, L. Tal-Or, S. Ferraz-Mello, S. Aigrain, M. Gillon, M. Endl: CoRoT: Harvest of the exoplanet program, *Icarus*, **226**, 1625–1634 (2013)

Nabert, C., K.-H. Glassmeier, F. Plaschke: A new method for solving the MHD equations in the magnetosheath, *Ann. Geophys.*, **31**, 419–437 (2013)

Nagai, T., I. Shinohara, S. Zenitani, R. Nakamura, T.K.M. Nakamura, M. Fujimoto, Y. Saito, T. Mukai: Three-dimensional structure of magnetic reconnection in the magnetotail from Geotail observations, *J. Geophys. Res.*, **118**, 1667–1678 (2013)

Nagai, T., S. Zenitani, I. Shinohara, R. Nakamura, M. Fujimoto, Y. Saito, T. Mukai: Ion and electron dynamics in the ion-electron decoupling region of magnetic reconnection with Geotail observations, *J. Geophys. Res.*, **118**, 7703–7713 (2013)

Nakamura, R., F. Plaschke, R. Teubenbacher, L. Giner, W. Baumjohann, W. Magnes, M. Steller, R.B. Torbert, H. Vaith, M. Chutter, K.-H. Fornaçon, K.-H. Glassmeier, C. Carr: Inter-instrument calibration using magnetic field data form Flux Gate Magnetometer (FGM) and Electron Drift Instrument (EDI) onboard Cluster, *Geosci. Instrum. Method. Data Syst. Disc.*, **3**, 459–487 (2013)

Nakamura, R., W. Baumjohann, E.V. Panov, M. Volwerk, J. Birn, A. Artemyev, A.A. Petrukovich, O. Amm, L. Juusola, M.V. Kubyshkina, S. Apatenkov, E.A. Kronberg, P.W. Daly, M. Fillingim, J.M. Weygand, A. Fazakerley, Y. Khotyaintsev: Flow bouncing and electron injection observed by Cluster, *J. Geophys. Res.*, **118**, 2055–2078 (2013)

Narita, Y., K.-H. Glassmeier, U. Motschmann, M. Wilczek: Doppler shift and broadening in solar wind turbulence, *Earth Planets Space*, **65**, e5–e8 (2013)

Narita, Y., R. Nakamura, W. Baumjohann: Cluster as current sheet surveyor in the magnetotail, *Ann. Geophys.*, **31**, 1605–1610 (2013)

Nordström, T., G. Stenberg, H. Nilsson, S. Barabash, T.L. Zhang: Venus ion outflow estimates at solar minimum: Influence of reference frames and disturbed solar wind conditions, *J. Geophys. Res.*, **118**, 3592–3601 (2013)

Ou, J.M., A. Du, E. Thebault, W.Y. Xu, X.B. Tian, T.L. Zhang: A high resolution lithospheric magnetic field model over China, *Sci. China D*, **56**, 1759–1768 (2013)

Panchenko, M., H.O. Rucker, W.M. Farrell: Periodic bursts of Jovian non-Io decametric radio emission, *Planet. Space Sci.*, **77**, 3–11 (2013)

Panov, E.V., A.V. Artemyev, W. Baumjohann, R. Nakamura, V. Angelopoulos: Transient electron precipitation during oscillatory BBF braking: THEMIS observations and theoretical estimates, *J. Geophys. Res.*, **118**, 3065–3076 (2013)

Panov, E.V., M.V. Kubyshkina, R. Nakamura, W. Baumjohann, V. Angelopoulos, V.A. Sergeev, A.A. Petrukovich: Oscillatory flow braking in the magnetotail: THEMIS statistics, *Geophys. Res. Lett.*, **40**, 2505–2510 (2013)

Panov, E.V., W. Baumjohann, R. Nakamura, O. Amm, M.V. Kubyshkina, K.-H. Glassmeier, J.M. Weygand, V. Angelopoulos, A.A. Petrukovich, V.A. Sergeev: Ionospheric response to oscillatory flow braking in the magnetotail, *J. Geophys. Res.*, **118**, 1529–1544 (2013)

Pérez-de-Tejada, H., R. Lundin, H. Durand-Manterola, S. Barabash, T.L. Zhang, J.A. Sauvaud, M. Reyes-Ruiz: Solar wind-driven plasma fluxes from the Venus ionosphere, *J. Geophys. Res.*, **118**, 7497–7506 (2013)

Perschke, C., Y. Narita, S.P. Gary, U. Motschmann, K.-H. Glassmeier: Dispersion relation analysis of turbulent magnetic field fluctuations in fast solar wind, *Ann. Geophys.*, **31**, 1949–1955 (2013)

Petrukovich, A.A., A.V. Artemyev, R. Nakamura, E.V. Panov, W. Baumjohann: Cluster observations of delta Bz / delta x during growth phase magnetotail stretching intervals, *J. Geophys. Res.*, **118**, 5720–5730 (2013)

Plaschke, F., H. Hietala, V. Angelopoulos: Anti-sunward high-speed jets in the subsolar magnetosheath, *Ann. Geophys.*, **31**, 1877–1889 (2013)

Plaschke, F., V. Angelopoulos, K.-H. Glassmeier: Magnetopause surface waves: THEMIS observations compared to MHD theory, *J. Geophys. Res.*, **118**, 1483–1499 (2013)

Popova, I., A. Rozhnoi, M. Solovieva, B. Levin, M. Hayakawa, Y. Hobara, P.F. Biagi, K. Schwingenschuh: Neural network approach to the prediction of seismic events based on low-frequency signal monitoring of the Kuril-Kamchatka and Japanese regions, *Ann. of Geophys.*, **56**, R0328 (2013)

Ramstad, R., Y. Futaana, S. Barabash, H. Nilsson, S.M. del Campo B., R. Lundin, K. Schwingenschuh: Phobos 2/ASPERA data revisited: Planetary ion escape rate from Mars near the 1989 solar maximum, *Geophys. Res. Lett.*, **40**, 477–481 (2013)

Romanelli, N., C. Bertucci, D. Gómez, C. Mazelle, M. Delva: Proton cyclotron waves upstream from Mars: Observations from Mars Global Surveyor, *Planet. Space Sci.*, **76**, 1–9 (2013)

Rong, Z.J., W.X. Wan, C. Shen, T.L. Zhang, A.T.Y. Lui, Y. Wang, M.W. Dunlop, Y.C. Zhang, Q.-G. Zong: Method for inferring the axis orientation of cylindrical magnetic flux rope based on single-point measurement, *J. Geophys. Res.*, **118**, 271–283 (2013)

Runov, A., V. Angelopoulos, C. Gabrielse, X.-Z. Zhou, D. Turner, F. Plaschke: Electron fluxes and pitch-angle distributions at dipolarization fronts: THEMIS multipoint observations, *J. Geophys. Res.*, **118**, 744–755 (2013)

Russell, C.T., H. Leinweber, R.A. Hart, H.Y. Wei, R.J. Strangeway, T.L. Zhang: Venus Express observations of ULF and ELF waves in the Venus ionosphere: Wave properties and sources, *Icarus*, **226**, 1527–1537 (2013)

Russell, C.T., H. Leinweber, T.L. Zhang, J.T.M. Daniels, R.J. Strangeway, H. Wei: Electromagnetic waves observed on a flight over a Venus electrical storm, *Geophys. Res. Lett.*, **40**, 216–220 (2013)

Sayanagi, K.M., U.A. Dyudina, S.P. Ewald, G. Fischer, A.P. Ingersoll, W.S. Kurth, G.D. Muro, C.C. Porco, R.A. West: Dynamics of Saturn's great storm of 2010–2011 from Cassini ISS and RPWS, *Icarus*, **223**, 460–478 (2013)

Shan, L.C., Q.M. Lu, T.L. Zhang, X.L. Gao, C. Huang, Y.Q. Su, S. Wang: Comparison between magnetic coplanarity and MVA methods in determining the normal of Venusian bow shock, *Chin. Sci. Bull.*, **58**, 2469–2472 (2013)

Shaposhnikov, V.E., V.V. Zaitsev, H.O. Rucker, G.V. Litvinenko: On ultraviolet emission observed on the flanks of Io, *J. Geophys. Res.*, **118**, 4248–4252 (2013)

Sharma, R., N. Srivastava, D. Chakrabarty, C. Möstl, Q. Hu: Interplanetary and geomagnetic consequences of 5 January 2005 CMEs associated with eruptive filaments, *J. Geophys. Res.*, **118**, 3954–3967 (2013)

Shi, J.K., Z. Wang, K. Torkar, M. Friedrich, X. Wang, C. Liu, Y.B. Guan, G.W. Zhu: Ionospheric E-F valley observed by a sounding rocket at the low-latitude station Hainan, *Ann. Geophys.*, **31**, 1459–1462 (2013)

Teh, W.-L., R. Nakamura, W. Baumjohann: Magnetic field topology of the plasma sheet boundary layer, *J. Geophys. Res.*, **118**, 4059–4065 (2013)

Torkar, K., M. Tajmar: Qualification of the liquid metal ion source instruments for the NASA MMS mission, *IEEE Trans. Plasma Sci.*, **41**, 3512–3519 (2013)

Török, T., M. Temmer, G. Valori, A.M. Veronig, L. van Driel-Gesztelyi, B. Vrsnak: Initiation of Coronal Mass Ejections by sunspot rotation, *Solar Phys.*, **286**, 453–477 (2013)

Treumann, R.A., W. Baumjohann: Collisionless magnetic reconnection in space plasmas, *Front. Physics*, **1**, 31 (2013)

Treumann, R.A., W. Baumjohann: Incomplete-exclusion statistical mechanics in violent relaxation, *Astron. Astrophys.*, **558**, A40 (2013)

Treumann, R.A., W. Baumjohann: Magnetic susceptibility from electron holes, *Ann. Geophys.*, **31**, 1191–1193 (2013)

Volwerk, M., C. Koenders, M. Delva, I. Richter, K. Schwingenschuh, M.S. Bentley, K.-H. Glassmeier: Corrigendum to "Ion cyclotron waves during the Rosetta approach phase: a magnetic estimate of cometary outgassing" published in Ann. Geophys., 31, 2201–2206, 2013, *Ann. Geophys.*, **31**, 2213 (2013)

Volwerk, M., C. Koenders, M. Delva, I. Richter, K. Schwingenschuh, M.S. Bentley, K.-H. Glassmeier: Ion cyclotron waves during the Rosetta approach phase: A magnetic estimate of cometary outgassing, *Ann. Geophys.*, **31**, 2201–2206 (2013)

Volwerk, M., N. Andre, C.S. Arridge, C.M. Jackman, X. Jia, S.E. Milan, A. Radioti, M.F. Vogt, A.P. Walsh, R. Nakamura, A. Masters, C. Forsyth: Comparative magnetotail flapping: An overview of selected events at Earth, Jupiter and Saturn, *Ann. Geophys.*, **31**, 817–833 (2013)

Volwerk, M., X. Jia, C. Paranicas, W.S. Kurth, M.G. Kivelson, K.K. Khurana: ULF waves in Ganymede's upstream magnetosphere, *Ann. Geophys.*, **31**, 45–59 (2013)

Wang, R., A. Du, R. Nakamura, Q. Lu, Y.V. Khotyaintsev, M. Volwerk, T.L. Zhang, E.A. Kronberg, P.W. Daly, A.N. Fazakerley: Observation of multiple sub-cavities adjacent to single separatrix, *Geophys. Res. Lett.*, **40**, 2511–2517 (2013)

Wu, M.Y., M. Volwerk, Q.M. Lu, Z. Vörös, R. Nakamura, T.L. Zhang: The proton temperature anisotropy associated with bursty bulk flows in the magnetotail, *J. Geophys. Res.*, **118**, 4875–4883 (2013)

Wu, M.Y., Q.M. Lu, M. Volwerk, Z. Vörös, T.L. Zhang, L.C. Shan, C. Huang: A statistical study of electron acceleration behind the dipolarization fronts in the magnetotail, *J. Geophys. Res.*, **118**, 4804–4810 (2013)

Yan, J., O. Baur, L. Fei, P. Jinsong: Long-wavelength lunar gravity field recovery from simulated orbit and inter-satellite tracking data, *Adv. Space Res.*, **52**, 1919–1928 (2013)

Yan, J., Z. Zhong, F. Li, J.M. Dohm, J. Ping, J. Cao, X. Li: Comparison analyses on the 150x 150 lunar gravity field models by gravity/topography admittance, correlation and precision orbit determination, *Adv. Space Res.*, **52**, 512–520 (2013)

Zaqarashvili, T.V., M.L. Khodachenko, R. Soler: Torsional Alfvén waves in partially ionized solar plasma: Effects of neutral helium and stratification, *Astron. Astrophys.*, **549**, A113 (2013)

Zaqarashvili, T.V., V.N. Melnik, A.I. Brazhenko, M. Panchenko, A.A. Konovalenko, A.V. Franzuzenko, V.V. Dorovskyy, H.O. Rucker: Radio seismology of the outer solar corona, *Astron. Astrophys.*, **555**, A55 (2013)

Zhang, Y.C., C. Shen, Z.X. Liu, Z.J. Rong, T.L. Zhang, A. Marchaudon, H. Zhang, S.P. Duan, Y.H. Ma, M.W. Dunlop, Y.Y. Yang, C.M. Carr, I. Dandouras: Two different types of plasmoids in the plasma sheet: Cluster multisatellite analysis application, *J. Geophys. Res.*, **118**, 5437–5444 (2013)

Zhong, J., Z.Y. Pu, M.W. Dunlop, Y.V. Bogdanova, X.G. Wang, C.J. Xiao, R.L. Guo, H. Hasegawa, J. Raeder, X.Z. Zhou, V. Angelopoulos, Q.G. Zong, S.Y. Fu, L. Xie, M.G.G.T. Taylor, C. Shen, J. Berchem, Q.H. Zhang, M. Volwerk, J.P. Eastwood: Three-dimensional magnetic flux rope structure formed by multiple sequential X-line reconnection at the magnetopause, *J. Geophys. Res.*, **118**, 1904–1911 (2013)

# Books

Lammer, H.: Origin and Evolution of Planetary Atmospheres. Implications for Habitability, Springer, Heidelberg, 98 pages (2013)

# Proceedings & Book Chapters

Arridge, C., A. Maier, A. Luntzer, R. Tlustos, B. Bonfond, S. Charnoz, C. Briois, N. Rambaux, M. Laneuville, N. Andr, R. Sallantin, T. Cavali, S. Hess, C. Briand, D. Gautier, L. Lamy, O. Mousis, B. Christophe, G. Tobie, A. Morschhauser, J. Hillier, M. Trielo, F. Neubauer, E. Grn, H. Krger, P. Strub, E. Roussos, J. Blum, K. Konstantinidis, F. Spahn, N. Nettelmann, E. Khalisi, A. Mocker, G. Moragas-Klosterbeyer, F. Postberg, R. Soja, R. Srama, V. Sterken, C. Labrianidis, I. Daglis, C. Bracken, S. McKenna-Lawlor, G. Filacchione, D. Grassi, D. Lucchesi, A. Milillo, R. Peron, F. Tosi, D. Turrini, H. Kimura, M. Costa-Sitja, T. Bocanegra-Bahamon, D. Dirkx, I. Gerth, J. Agarwal, C. Agnor,

C. Jackman, J. Mac Arthur, J. Nordheim, R. Ambrosi, S. Badman, H. Melin, T. Stallard, R. Holme, L. Fletcher, D. Ban eld, M. Hedman, M. Tiscareno, A. Rymer, E. Turtle, M. Horanyi, S. Hsu, S. Kempf, Z. Sternovsky, R. Wilson, S. Brooks, J. Castillo-Rogez, M. Hofstadter, K. Retherford, J. Moses, C. Russell, G. Hospodarsky: The science case for an orbital mission to Uranus. In: *Cosmic Vision. White Papers submitted in response to ESA's Call for Science Themes for the L2 and L3 Missions*, ESA, Noordwijk, 499-518 (2013)

Besser, B.P., H.I.M. Lichtenegger, K. Schwingenschuh, H.-U. Eichelberger, M. Stachel: General approach to solutions of ionospheric cavity wave propagation problems. In: *Juan Antonio Morente Chiquero: In Memoriam*, Eds. Carrion Perez, M.C., A. Delgado Mora, R. Hidalgo Alvarez, A. Martin Molina, F.J. Olmo Reyes, J.L. Ortega Vinuesa, J. Porti Duran, Universidad de Granada, Granada, Spain, 51-60 (2013)

Boudjada, M.Y., F.P. Biagi, S. Sawas, K. Schwingenschuh, M. Parrot, G. Stangl, P. Galopeau, B.P. Besser, G. Prattes, W. Voller: Analysis of sub-ionospheric transmitter signal behaviours above L'Aquila region. In: *Thales. In Honor of Professor Emeritus Michael E. Contadakis*, Eds. Arabelos, D., C. Kaltsikis, S. Spatalas, I.N. Tziavos, ZITI, Tessaloniki, 142-149 (2013)

Broeg, C., A. Fortier, D. Ehrenreich, Y. Alibert, W. Baumjohann, W. Benz, M. Deleuil, M. Gillon, A. Ivanov, R. Liseau, M. Meyer, G. Oloffson, I. Pagano, G. Piotto, D. Pollacco, D. Queloz, R. Ragazzoni, E. Renotte, M. Steller, N. Thomas, CHEOPS Team (http://cheops. unibe. ch/index. php/contact): CHEOPS: A transit photometry mission for ESA's small mission programme. In: *EPJ Web of Conferences*, EDP Sciences, Les Ulis Cedex, 03005 (2013)

Bruyninx, C., H. Habrich, A. Kenyeres, W. Söhne, G. Stangl, C. Völksen: EUREF Permanent Network. In: *International GNSS Technical Report 2012*, Eds. Dach, R., Y. Jean, IGS Central Bureau, Pasadena, 101-109 (2013)

Friedrich, M., K. Torkar, S. Robertson, S. Dickson: Bonus results from ion probes. In: *Proc. "21st ESA Symposium on European Rocket and Balloon Programmes and Related Research"*, Ed. Ouwehand, L., ESA, Noordwijk, 75-80 (2013)

Höggerl, N., E. Imrek, E. Zahn, G. Stangl, H.-P. Ranner: EUREF 13: National Report of Austria. In: *Proc. EUREF 2013 Budapest*, EUREF, Budapest, 5 (2013)

Iber, W.M., H. Knoll, B.P. Besser: Forschung - Technik - (Rüstungs-)Industrie. In: *Wirtschaft. Macht. Geschichte. Brüche und Kontinuitäten im 20. Jahrhundert. Festschrift Stefan Karner*, Eds. Schöpfer, G., B. Stelzl-Marx, Böhlau, Wien, 461-476 (2013)

Khodachenko, M.L., I.I. Alexeev, E.S. Belenkaya, H. Lammer: Magnetodisk-dominated magnetospheres of close orbit giant exoplanets. In: *EAS Publications Series 58, European Conference on Laboratory Astrophysics*, Cambridge University Press, Cambridge, UK, 233-237 (2013)

Lammer, H., K.G. Kislyakova, M. Güdel, M. Holmström, N.V. Erkaev, P. Odert, M.L. Khodachenko: Stability of Earth-like N2 atmospheres: Implications for habitability. In: *The Early Evolution of the Atmospheres of Terrestrial Planets, Astrophysics and Space Science Proceedings, 37*, Eds. Trigo-Rodriguez, J.M., F. Raulin, C. Muller, C. Nixon, Springer, New York, 33-52 (2013)

Pany, T., N. Falk, B. Riedl, C. Stöber, J. Winkel, H.-P. Ranner: GNSS synthetic aperture processing with artificial antenna motion. In: *Proceedings of ION GNSS+*, Institute of Navigation, Manassas, VA, USA, 9 p. (2013)

Ranner, H.-P., G. Stangl, T. Pany, D. Llorens del Rio, V.V. Denisenko: A multipath test bed for displacement synthetic aperture GNSS antennas. In: *CD-Proceedings of 4th International Galileo Science Colloquium*, ESA, Noordwijk, 7 p. (2013)

Stangl, G.: Tropospheric Zenith Delays for Trafelberg at extreme Conditions. In: *Jahrbuch Conrad Observatorium 2013*, Ed. ZAMG, ZAMG, Wien, 5 (2013)

Sünkel, H.: Satellitengeodäsie und Weltraumforschung. In: *Lebenszeugnisse österreichischer Vizekanzler: Das politische System*, Ed. Mantl, W., Böhlau, Wien, n - n+6 (2013)

Torkar, K.: Kometenstaub als Geheimnisträger des Sonnensystems. Das Staubmikroskop MIDAS auf Mission zum Kometen Tschurjumow-Gerasimenko. In: *Staub. Eine interdisziplinäre Perspektive*, Eds. Gethmann, D., A. Wagner, LIT Verlag, Wien, 161-182 (2013)

Volwerk, M.: The Earth's magnetotail as a plasma physics laboratory: A Cluster perspective. In: *370 Years of Astronomy in Utrecht. ASP Conference Series, Vol. 470*, Eds. Pugliese, G., A. de Koter, M. Wijburg, Astronomical Society of the Pacific, Orem, Utah, USA, 227–229 (2013)

For oral presentations and posters please refer to www.iwf.oeaw.ac.at/en/publications.

# Personnel

Alexandrova, Alexandra, MSc (P)
Al-Ubaidi, Tarek, Dipl.-Ing. (P)
Arkhypov, Oleksiy, Dr. (P)
Aydogar, Özer, Dipl.-Ing. (E)
Baumjohann, Wolfgang, Prof. (E)
Baur, Oliver, Dr. (S)
Bentley, Mark, Dr. (P)
Berghofer, Gerhard, Ing. (E)
Besser, Bruno P., Dr. (E)
Boakes Peter, Dr. (P)
Boudjada, Mohammed Y., Dr. (P)
Bourdin, Philippe, Dr. (E)
Delva, Magda, Dr. (E)
Dwivedi, Navin, Dr. (E)
Eichelberger, Hans U., Dipl.-Ing. (E)
Fischer, David, Dipl.-Ing. (E)
Fischer, Georg, Dr. (P)
Flock, Barbara, Mag. (A)
Fremuth, Gerhard, Dipl.-Ing. (E)
Giner, Franz, Dipl.-Ing. (E)
Graf, Christian, Ing. (S)
Grill, Claudia (A)
Hagen, Christian, Dipl.-Ing. (E)
Hasiba, Johann, Dipl.-Ing. (E)
Hofmann, Karl, Dipl.-Ing. (E)
Höck, Eduard, Dipl.-Ing. (S)
Hradecky, Doris (A)
Jernej, Irmgard, Ing. (E)
Jeszenszky, Harald, Dipl.-Ing. (E)
Juvan, Ines (P)
Kapper, Michael, Dr. (P)
Kargl, Günter, Dr. (P)
Khodachenko, Maxim L., Dr. (P)
Kiehas, Stefan, Dr. (P)
Kirchner, Georg, Dr. (S)
Kislyakova, Kristina, Dr. (P)
Koidl, Franz, Ing. (S)
Korovinskiy, Daniil, Dr. (P)
Kömle, Norbert I., Doz. (P)
Krauss, Sandro, Dr. (S)
Kürbisch, Christoph, Ing. (E)
Laky, Gunter, Dipl.-Ing. (E)
Lammer, Helmut, Dr. (P)
Leichtfried, Mario, Ing. (E)
Leitner, Stefan, Dipl.-Ing. (E)
Lichtenegger, Herbert I.M., Dr. (E)
Macher, Wolfgang, Dr. (P)
Magnes, Werner, Dr. (E)
Maier, Andrea, Dipl.-Ing. (S)
Močnik, Karl, Dr. (E)
Nakamura, Rumi, Doz. (P)
Narita, Yasuhito, Doz. (E)
Neukirchner, Sonja, Ing. (E)
Nischelwitzer-Fennes, Ute, Ing. (E)
Ottacher, Harald, Dipl.-Ing. (E)
Pagaran, Joseph A., Dr. (P)
Panchenko, Mykhaylo, Dr. (P)
Panov, Evgeny, Dr. (E)
Pfleger, Martin, Dr. (S)
Pitterle, Martin (A)
Plaschke, Ferdinand, Dr. (E)
Pollinger, Andreas, Dr. (E)
Prattes, Gustav, Dipl.-Ing. (E)
Rucker, Helmut O., Prof. (P)
Sasunov, Jury, Dr. (P)
Scherf, Manuel, Mag. (P)
Scherr, Alexandra, Mag. (A)
Schmid, Daniel, Dipl.-Ing. (P)
Stachel, Manfred, Dipl.-Ing. (A)
Stangl, Günter, Dr. (S, BEV)
Steinberger, Michael, Dipl.-Ing. (E)
Steller, Manfred B., Dr. (E)
Stieninger, Reinhard, Ing. (S)
Sünkel, Hans, Prof. (S, BMWF)
Teh, Wai-Leong, Dr. (P)
Topf, Florian, BSc (P)
Valavanoglou, Aris, Dipl.-Ing. (E)
Voller, Wolfgang G., Mag. (P)
Volwerk, Martin, Dr. (E)
Vörös, Zoltán, Dr. (P)
Wallner, Robert, Ing. (E)
Weber, Christof, Mag. (P)
Wirnsberger, Harald, Dipl.-Ing. (S)
Yamamoto, Keiko, Dr. (S)
Zaqarashvili, Teimuraz, Dr. (P)
Zehetleitner, Sigrid, Mag. (A)
Zhang, Tie-Long, Prof. (E)

As of 31 December 2013

E: Experimental Space Research
P: Extraterrestrial Physics
S: Satellite Geodesy
A: Administration
BEV: Federal Office for Metrology and Surveying
BMWF: Federal Ministry for Science and Research

## Impressum

Published by
IWF Director



Compiled and designed by
IWF Public Relations

Printed by
Druckwerk, 8020 Graz

Institut für Weltraumforschung (IWF)
Österreichische Akademie der Wissenschaften (ÖAW)
Schmiedlstraße 6
8042 Graz, Austria
T +43 316 4120-400
pr.iwf@oeaw.ac.at
iwf.oeaw.ac.at
@IWF_Graz